Finite-temperature quasicontinuum method for multiscale analysis of silicon nanostructures

Z. Tang, H. Zhao, G. Li, and N. R. Aluru
Department of Mechanical Science and Engineering, Beckman Institute for Advanced Science and Technology, University of Illinois at Urbana-Champaign, Illinois 61801, USA
(Received 22 December 2005; revised manuscript received 1 April 2006; published 23 August 2006)

In this paper, we extend the quasicontinuum approach for a multiscale analysis of silicon nanostructures at finite temperature. The quasicontinuum method uses the classical continuum mechanics framework, but the constitutive response of the system is determined by employing an atomistic description. For finite-temperature solid systems under isothermal conditions, the constitutive response is determined by using the Helmholtz free energy density. The static part of the Helmholtz free energy density is obtained directly from the interatomic potential while the vibrational part is calculated by using the theory of quantum-mechanical lattice dynamics. Specifically, we investigate three quasiharmonic models, namely the real space quasiharmonic model, the local quasiharmonic model, and the reciprocal space quasiharmonic model, to compute the vibrational free energy. Using the finite-temperature quasicontinuum method, we compute the effect of the temperature and strain on the phonon density of states, phonon Grüneisen parameters, and the elastic properties of the Tersoff silicon. We also compute the mechanical response of silicon nanostructures for various external loads and the results are compared to molecular dynamics simulations.

DOI: 10.1103/PhysRevB.74.064110 PACS number(s): 46.15.−x, 62.25.+g, 02.70.−c

I. INTRODUCTION

Rapid advances in nanotechnology have led to the fabrication of nanoscale mechanical structures with applications in nanoelectromechanical systems (NEMS).[1–3] The design, optimization, and fabrication of NEMS for various applications can be accelerated by developing accurate physical theories and computational design tools that describe the motion and operation of nanostructures.[4,5] There are two major challenges in the physical modeling and computational analysis of nanostructures. First, when the characteristic length of NEMS scales down to several tens of nanometers, nanoscale effects, such as quantum effects, material defects, and surface effects become significant. Classical theories based on continuum assumptions or the computational design tools that have been developed for microsystems and macrosystems may not be directly applicable for nanosystems because of the small scales encountered in NEMS. Second, although the characteristic length of NEMS is often a few nanometers, the entire system could still be of the order of micrometers. Therefore, typical NEMS can still contain millions of atoms. In this case, atomistic simulation methods such as *ab initio* calculations, molecular dynamics (MD), and Monte Carlo (MC) simulations, that can be employed for an accurate analysis of systems comprising several hundreds of atoms, are computationally impractical for design and optimization of practical NEMS.

To achieve the goal of accurately capturing the atomistic physics and yet retaining the efficiency of continuum models, multiscale modeling and simulation techniques which connect and integrate the atomistic and continuum theories have recently attracted considerable research interest.[6–21] Broadly defined, there are three multiscale modeling strategies: direct coupling, top-down, and bottom-up approaches. Direct coupling methods[6–10] typically decompose the physical domain into atomistic, continuum, and interface regions. Atomistic and continuum calculations are performed separately and the interface regions are used to exchange information between the atomistic and continuum regions. Top-down approaches, such as the quasicontinuum (QC) method,[11–13] the bridging scale method,[14] and the heterogeneous multiscale method,[15] solve the continuum equations by extracting constitutive laws from the underlying atomistic descriptions. In contrast, bottom-up methods such as the coarse-grained molecular dynamics[16] and multigrid bridging approaches[17] coarse-grain the atoms of the system into macroatoms and the fundamental equations defined on the atoms are coarse-grained into equivalent macroscale equations. Of these multiscale modeling techniques, the QC approach is attractive due to its simplicity and generality. The QC method[11–13] was originally formulated using a continuum finite element framework and restricted to zero temperature. To accurately predict the mechanical behavior of nanosystems, it is necessary to take into account the effect of finite temperature. Recently, the QC approach has been extended to deal with finite-temperature solid systems.[18–21] In Refs. 18 and 19, a QC Monte Carlo (QCMC) method and a QC free energy minimization (QCFEM) method were proposed to study equilibrium properties of defects at finite temperature. In these methods, a local quasiharmonic approximation[22] of the interatomic potential was used to compute the entropic energy contribution from the thermal vibration of the atoms. The entropic energy contribution was then added to the zero temperature QC energy to construct the effective energy and the free energy in the QCMC and QCFEM methods, respectively. In Ref. 20, a finite-temperature QC method was proposed to investigate the thermal and mechanical properties of single-wall carbon nanotubes, where the local quasiharmonic approximation of the Brenner's potential was employed to compute the Helmholtz free energy density of carbon atoms. In Ref. 21, the QC concepts are employed to develop a coarse-grained alternative to molecular dynamics. The thermal vibrational part of the coarse-grained potential energy is obtained from the local quasiharmonic approximation.

In this paper, within the top-down framework, we provide an alternative approach to extend the QC method to perform a mechanical analysis of nanostructures at finite-temperature. In particular, we formulate a finite-temperature QC method to calculate the mechanical response of silicon nanostructures subjected to externally applied forces. We solve the continuum elasticity governing equations, but extract the material constitutive laws using an underlying atomistic description where the silicon atoms are described by the Tersoff interatomic potential.[23] At finite temperature, for an isothermal system, the constitutive relations are computed by using the Helmholtz free energy density of the representative atoms. The static part of the Helmholtz free energy density is obtained directly from the Tersoff interatomic potential while the vibrational part (or the finite temperature part) is calculated by using the quantum-mechanical lattice dynamics. In this paper, we employ three quasiharmonic models, namely the real space quasiharmonic (QHM) model, the local quasiharmonic (LQHM) model, and the reciprocal space (or **k**-space) quasiharmonic (QHMK) model, to compute the vibrational Helmholtz free energy density. For Tersoff silicon, we calculate the temperature and strain effects on the phonon density of states (PDOS), phonon Grüneisen parameters, and the elastic properties. By comparing the results obtained from the three quasiharmonic models to experimental and MD results, we observe that (1) the QHM model predicts the material properties accurately, however, it is extremely inefficient when the system contains more than several hundred atoms; (2) the LQHM model is simple and efficient, but it can be inaccurate in predicting elastic constants of Tersoff silicon, especially when the material is under strain; (3) the QHMK model can predict the material properties accurately and efficiently. Based on these observations, we propose to employ the QHMK model along with a semilocal approximation of the vibrational Helmholtz free energy density to extract the material properties. We then compute the mechanical response of silicon nanostructures subjected to various external loads by using the proposed finite-temperature QC method. We also perform MD simulations for the mechanical analysis of the silicon nanostructures and compare the results with the finite-temperature QC method. It is shown that, for silicon nanostructures larger than a few nanometers, the QHMK model predicts the mechanical response of the nanostructure accurately over a large temperature range, while the LQHM model can be inaccurate for Tersoff silicon.

The rest of the paper is organized as follows. Section II presents the finite-temperature QC method, Sec. III describes the molecular dynamics simulations used in this paper, Sec. IV presents results on the material properties and mechanical analysis of silicon nanostructures, and Sec. V presents conclusions.

II. THEORY

The key idea in the QC approach is to adopt the framework of continuum mechanics, but to extract the material properties and the constitutive relations from the atomistic description of the underlying local environment. Figure 1 illustrates the basic idea in the QC approach by using a simple example: a silicon structure subjected to a uniaxial external force. In the QC approach, the structure is described in two levels: the continuum level and the atomistic level. In the continuum level, the structure is represented by a set of discrete nodes or elements and the deformation of the structure is determined by the laws of continuum mechanics. In the atomistic level, the crystalline silicon structure consists of atoms which are connected by covalent bonds and each atom is tetrahedrally bonded to four neighboring silicon atoms, as shown in Fig. 1. When the structure is subjected to an external force, the configuration of the silicon atoms changes to balance the external force. The change in position of the atoms in the crystal lattice manifests as deformation at the continuum level. In the QC approach, the material volume surrounding each continuum node corresponds to a large number of atoms in the atomistic scale as shown in Fig. 1 and the covalent bonding of the atoms is described by atomistic models, e.g., empirical interatomic potentials and tight-binding descriptions.[12,24] At the continuum level, the governing equations can be solved by using a variety of numerical methods. The deformation gradient at each continuum node is used in the underlying crystal lattice (in accordance with the Cauchy-Born rule[25]) to determine the deformed configuration of the atoms. The material constitutive relations of the continuum nodes are then extracted from the underlying crystal lattice. Based on the above description, the QC approach can be classified as a "top-down" multiscale strategy.

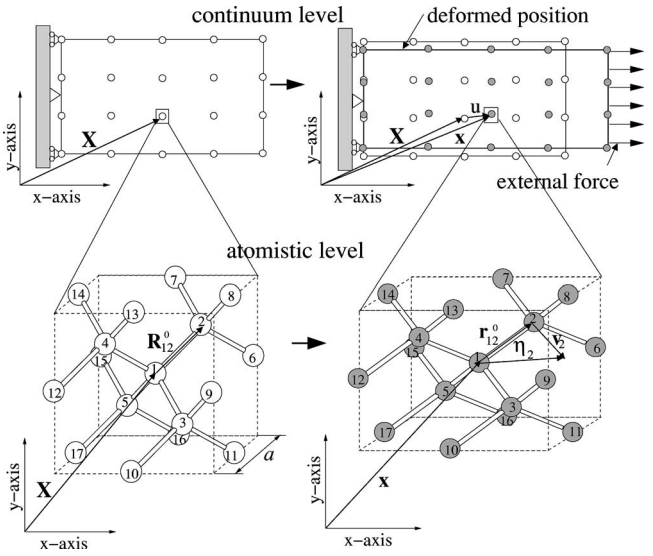

FIG. 1. The two-level paradigm of the QC approach: at the continuum level, the structure is represented by a set of discrete nodes and each node corresponds to a large number of silicon atoms at the atomistic level. Note that although only 17 atoms are shown for the continuum node in the figure, the actual number of atoms represented by the node can be much larger. When the structure deforms due to an external force, the equilibrium position of the atoms of the underlying crystal lattice changes to balance the external force.

In the original QC method,[11–13] where no temperature is considered (i.e., $T=0$ K), the mechanical response of the at-

oms and, consequently, the constitutive laws of the material at the continuum nodes are solely determined by the interatomic potential energy of the atoms. In the case of finite temperature, the crystal structure is a thermodynamic system and the mechanical response of the system depends on the thermodynamic quantities such as the internal energy (for the adiabatic system) or the Helmholtz free energy (for the isothermal system).[26] The constitutive relations for the continuum nodes are obtained from the internal energy or the Helmholtz free energy density. The internal energy or the Helmholtz free energy is extracted from the atomic lattice by using the theory of quantum-mechanical lattice dynamics. Several lattice dynamics models based on the quasiharmonic approximation of the interatomic potential are discussed in this paper.

Before proceeding to the details on the finite-temperature QC approach, we introduce the notation used in this paper. As shown in Fig. 1, at the continuum level, the initial and the deformed positions of a continuum node are denoted by $\mathbf{X}$ and $\mathbf{x}$, respectively. The displacement of the node is denoted by $\mathbf{u}$ with the relation $\mathbf{x}=\mathbf{X}+\mathbf{u}$. At the atomistic level, as shown in Fig. 1, the initial and the deformed *equilibrium* position of the center atom 1, which is the representative atom corresponding to the continuum node, are denoted by $\mathbf{X}$ and $\mathbf{x}$, respectively. The vectors between the equilibrium positions of atoms 1 and 2 in the initial and the deformed configurations are denoted by $\mathbf{R}_{12}^0$ and $\mathbf{r}_{12}^0$, respectively. At finite temperature, the atom fluctuates around its equilibrium position. The thermal vibrational displacements of atoms 1 and 2 are denoted by $\mathbf{v}_1$ and $\mathbf{v}_2$, respectively. Note that, for clarity, the thermal vibrational displacements are only shown in the deformed configuration in Fig. 1. The instantaneous positions of atoms 1 and 2, denoted by $\mathbf{x}_1$ and $\mathbf{x}_2$, in the deformed configuration are given by

$$\mathbf{x}_1 = \mathbf{x} + \mathbf{v}_1, \tag{1}$$

$$\mathbf{x}_2 = \mathbf{x} + \mathbf{r}_{12}^0 + \mathbf{v}_2. \tag{2}$$

Denoting the vectors from the equilibrium position of atom 1 (in the deformed configuration) to the instantaneous position and equilibrium position of an atom α ($\alpha=1,2,\ldots$) by $\boldsymbol{\eta}_\alpha$ and $\boldsymbol{\eta}_\alpha^0$, respectively, we obtain

$$\boldsymbol{\eta}_\alpha = \mathbf{x}_\alpha - \mathbf{x}, \tag{3}$$

$$\boldsymbol{\eta}_\alpha^0 = \mathbf{r}_{1\alpha}^0. \tag{4}$$

Note that $\boldsymbol{\eta}_1^0=\mathbf{r}_{11}^0=0$. At any instant, the distance between atom α and atom β, denoted by $r_{\alpha\beta}$, is given by

$$r_{\alpha\beta} = |\mathbf{r}_{\alpha\beta}| = |\mathbf{x}_\beta - \mathbf{x}_\alpha| = |\boldsymbol{\eta}_\beta - \boldsymbol{\eta}_\alpha|, \tag{5}$$

where $\mathbf{r}_{\alpha\beta}$ is the vector between the instantaneous positions of atoms α and β. At finite temperature, the vector, $\mathbf{R}_{\alpha\beta}^0$, between the equilibrium positions of atoms α and β in the initial configuration is given by

$$\mathbf{R}_{\alpha\beta}^0 = \frac{a\bar{\mathbf{R}}_{\alpha\beta}}{\bar{a}}, \tag{6}$$

where a is the lattice constant at a given temperature, $\bar{a}$ is the 0 K static lattice constant (i.e., neglecting thermal fluctuation), and $\bar{\mathbf{R}}_{\alpha\beta}$ is the vector between atoms α and β in the initial configuration at 0 K.

A. Continuum level description

The continuum elastostatic governing equations for an arbitrary domain Ω are given by[27]

$$\nabla\cdot(\mathbf{FS}) + \mathbf{B} = \mathbf{0} \quad \text{in } \Omega, \tag{7}$$

$$\mathbf{u} = \bar{\mathbf{G}} \quad \text{on } \Gamma_g, \tag{8}$$

$$\mathbf{P}\cdot\mathbf{N} = \bar{\mathbf{T}} \quad \text{on } \Gamma_h, \tag{9}$$

where $\mathbf{u}$ is the displacement vector of a continuum node from the initial configuration $\mathbf{X}$ to the deformed configuration $\mathbf{x}$ and $\mathbf{F}$ is the deformation gradient, which is given by $\mathbf{F}=\mathbf{I}+\partial\mathbf{u}/\partial\mathbf{X}$, where $\mathbf{I}$ is the identity tensor, $\mathbf{S}$ is the second Piola-Kirchhoff stress tensor, $\mathbf{N}$ is the unit outward normal vector in the initial configuration, $\mathbf{B}$ is the body force vector per unit undeformed volume, $\bar{\mathbf{G}}$ is the prescribed displacement vector on the boundary portion Γ_g, $\bar{\mathbf{T}}$ is the surface traction vector per unit undeformed area on the boundary Γ_h, and $\mathbf{P}$ is the first Piola-Kirchhoff stress tensor given by $\mathbf{P}=\mathbf{FS}$. In continuum mechanics, the second Piola-Kirchhoff stress $\mathbf{S}$ can be described by

$$\mathbf{S} = \frac{dW}{d\mathbf{E}}, \tag{10}$$

where W is the strain energy density function and $\mathbf{E}$ is the Green-Lagrange strain tensor, which is given by $\mathbf{E}=\frac{1}{2}(\mathbf{F}^T\mathbf{F}-\mathbf{I})$. Note that Eq. (10) is the general form of the constitutive law describing the material response to external forces. Depending on the form of the strain energy density function, different classes of materials can be defined. In classical continuum mechanics, analytical formulations of the strain energy density function have been developed for linear and nonlinear elastic, hyperelastic, and other types of materials.[27] Given a strain energy density function, the elastic constants can be obtained as

$$\mathbf{C}_{ijkl} = \frac{d\mathbf{S}_{ij}}{d\mathbf{E}_{kl}} = \frac{d^2W}{d\mathbf{E}_{ij}d\mathbf{E}_{kl}}, \quad i,j,k,l = 1,2,3. \tag{11}$$

The divergence of the first Piola-Kirchhoff stress tensor in the governing equation, Eq. (7), is thus given by

$$\nabla\cdot\mathbf{P} = \frac{\partial\mathbf{P}_{ij}}{\partial\mathbf{X}_j} = \frac{\partial\mathbf{F}_{ik}}{\partial\mathbf{X}_j}\mathbf{S}_{kj} + \mathbf{F}_{ik}\frac{\partial\mathbf{S}_{kj}}{\partial\mathbf{X}_j}$$
$$= \frac{\partial\mathbf{F}_{ik}}{\partial\mathbf{X}_j}\mathbf{S}_{kj} + \mathbf{F}_{ik}\mathbf{C}_{kjlm}\frac{\partial\mathbf{E}_{lm}}{\partial\mathbf{X}_j}, \quad i,j,k,l,m = 1,2,3. \tag{12}$$

Equations (7)–(12) provide a description of the elastostatic behavior of solid structures at the continuum level. For nanostructures, however, the use of continuum constitutive laws can be questionable, since both the form and the material properties in the constitutive laws can vary spatially due to material inhomogeneities and device geometry. To overcome this limitation, in the QC approach, the stress-strain relations, Eq. (10), are obtained directly from the underlying crystal lattice, i.e., by using an atomistic level description of the structure.

B. Atomistic level description

We use the Tersoff potential model[23] for a microscopic description of silicon in this work. The Tersoff potential has been used extensively to investigate the energetics and elastic properties of crystalline silicon.[28] In the Tersoff empirical potential model, the total lattice potential energy is expressed as the sum of local many-body interactions. The total potential energy U of the system is given by

$$U = \sum_{\alpha} U_{\alpha} = \frac{1}{2} \sum_{\alpha \neq \beta} V_{\alpha\beta}, \tag{13}$$

where α and β are the atom indices, U_{α} is the potential energy of atom α, and $V_{\alpha\beta}$ is the bond energy between atoms α and β and is given by

$$V_{\alpha\beta} = f_C(r_{\alpha\beta})[Ae^{-\lambda_1 r_{\alpha\beta}} - b_{\alpha\beta} Be^{-\lambda_2 r_{\alpha\beta}}], \tag{14}$$

where $r_{\alpha\beta}$ is the distance between atoms α and β, A is the coefficient of the repulsive term, B is the coefficient of the attractive term, λ_1 and λ_2 are constants, f_C is the cutoff function which has the form

$$f_C(r) = \begin{cases} 1 & r < R - D \\ \frac{1}{2} - \frac{1}{2} \sin[\pi(r-R)/2D] & R - D \leq r \leq R + D \\ 0 & r > R + D \end{cases}, \tag{15}$$

where R and D are constants, the function $b_{\alpha\beta}$ is a measure of the bond order which describes the dependence of the bond-formation energy on the local atomic arrangement due to the presence of other neighboring atoms, and is given by

$$b_{\alpha\beta} = (1 + \mu^n \zeta_{\alpha\beta}^n)^{-1/2n}, \tag{16}$$

$$\zeta_{\alpha\beta} = \sum_{\gamma \neq \alpha,\beta} f_C(r_{\alpha\gamma}) g(\cos\theta_{\alpha\beta\gamma}) e^{\lambda_3^3 (r_{\alpha\beta} - r_{\alpha\gamma})^3}, \tag{17}$$

$$g(\cos\theta) = 1 + c^2/d^2 - c^2/[d^2 + (h - \cos\theta)^2], \tag{18}$$

where γ denotes an atom other than α and β, $\zeta_{\alpha\beta}$ is called the effective coordination number, $\theta_{\alpha\beta\gamma}$ is the bond angle between the bonds $\alpha\beta$ and $\alpha\gamma$, and $g(\cos\theta)$ is the stabilization function of the tetrahedral structure. The remaining variables are constants. While several different parameter sets have been presented for the Tersoff model, the parameter values from Ref. 23 are used in this work.

C. QC method at classical zero temperature

In this paper, in the continuum level description of a silicon nanostructure, the structure is represented by a set of discrete continuum nodes and a continuum mechanical description of the structure is given by quantities such as the stress **S**, and the strain **E**, which are functions of the deformation gradient **F**. From a microscopic point of view, each continuum node is associated with an underlying crystal lattice consisting of silicon atoms bonded in the form of a diamond structure. When the macroscale structure deforms, the underlying lattice deforms accordingly. The interactions among the atoms in the underlying lattice are described by the Tersoff model, which takes into account the actual atom configuration at a given location and provides a description of the material behavior. To connect the macroscopic level description of the continuum nodes with the atomistic description of the underlying crystal lattice, we employ the hypotheses of the Cauchy-Born rule,[25] which states that the crystal lattice surrounding a continuum node is homogeneously distorted according to the deformation gradient at the continuum node. In addition, there exist additional inner displacements for the two interpenetrating fcc Bravais lattices (denoted by B_1 and B_2) of silicon crystal. For example, atoms 1 and 6–17 shown in Fig. 1 belong to one Bravais lattice and atoms 2–5 belong to the other Bravais lattice. In this paper, the inner displacements associated with B_1 and B_2 are denoted by $\boldsymbol{\xi}_1$ and $\boldsymbol{\xi}_2$, respectively. The Cauchy-Born rule can be expressed as

$$\mathbf{r}^0_{\alpha\beta} = \mathbf{F}\mathbf{R}^0_{\alpha\beta} + \boldsymbol{\xi}_j - \boldsymbol{\xi}_i, \quad \alpha \in B_i; \quad \beta \in B_j; \quad i,j = 1,2, \tag{19}$$

where $\boldsymbol{\xi}_i$, $i=1,2$, are the additional inner displacements of the two Bravais lattices which can be determined by the energy minimization for a given deformation gradient **F**. Since the inner displacements $\boldsymbol{\xi}_1$ and $\boldsymbol{\xi}_2$ are relative displacements between the two Bravais lattices, in order to rule out rigid-body translations we fix the lattice by setting $\boldsymbol{\xi}_2 = 0$. Therefore, $\boldsymbol{\xi}_2$ can be simply discarded. To simplify the notation, $\boldsymbol{\xi}_1$ is denoted as $\boldsymbol{\xi}$ in the rest of the paper. The Cauchy-Born rule can then be rewritten as

$$\mathbf{r}^0_{\alpha\beta} = \mathbf{F}\mathbf{R}^0_{\alpha\beta} + \boldsymbol{\xi} \quad \text{if } \alpha \in B_2 \text{ and } \beta \in B_1, \tag{20}$$

$$\mathbf{r}^0_{\alpha\beta} = \mathbf{F}\mathbf{R}^0_{\alpha\beta} - \boldsymbol{\xi} \quad \text{if } \alpha \in B_1 \text{ and } \beta \in B_2, \tag{21}$$

$$\mathbf{r}^0_{\alpha\beta} = \mathbf{F}\mathbf{R}^0_{\alpha\beta} \quad \text{if } \alpha,\beta \in \text{ same Bravais lattice}. \tag{22}$$

When the temperature is 0 K and the system is considered as a classical system, there is no thermal fluctuation of the atoms (i.e., $\mathbf{v}_i = 0$, $i=1,2,\ldots$, as shown in Fig. 1) and the strain energy density function in Eq. (10) is simply the potential energy per unit volume of the silicon lattice. Due to the symmetric properties of the diamond structure silicon lattice and as the Tersoff potential only includes the nearest neighbor interactions, the calculation of the strain energy density function and its derivatives can be limited to within a five-atom unit cell (see Fig. 1 in Ref. 29 for the five-atom unit cell) where, without losing generality, the four outer atoms are assumed to belong to the first fcc Bravais lattice B_1, and

the center atom belongs to the second fcc Bravais lattice B_2. The strain energy density, thus, can be rewritten as

$$W = W_U = \frac{U_1}{V_A} = \frac{1}{2V_A}\sum_{\beta=2}^{5} V_{1\beta}, \tag{23}$$

where W_U is the potential energy density, U_1 is the potential energy of the center atom which is numbered as 1, and V_A is the volume of an atom in the initial configuration, which is given by $a^3/8$, where a is the silicon lattice constant. Note that $a=\bar{a}=5.432$ Å for Tersoff silicon at classical 0 K.[28] In Eqs. (14)–(18), $V_{1\beta}$ is a function of the distances between the atoms at their instantaneous positions. At zero temperature, since $\mathbf{r}_{\alpha\beta}=\mathbf{r}^0_{\alpha\beta}$, Eqs. (14)–(18) can be combined as

$$V_{1\beta} = f_C(r^0_{1\beta})\left\{Ae^{-\lambda_1 r^0_{1\beta}} - Be^{-\lambda_2 r^0_{1\beta}}\left[1+\mu^n\left(\sum_{\gamma\neq 1,\beta} f_C(r^0_{1\gamma})g(\cos\theta^0_{1\beta\gamma})e^{\lambda_3^3(r^0_{1\beta}-r^0_{1\gamma})^3}\right)^n\right]^{-1/2n}\right\}, \tag{24}$$

where $\cos\theta^0_{1\beta\gamma}=[(r^0_{1\beta})^2+(r^0_{1\gamma})^2-(r^0_{\beta\gamma})^2]/(2r^0_{1\beta}r^0_{1\gamma})$. By using the Cauchy-Born rule given in Eqs. (20)–(22), one obtains

$$r^0_{1\beta} = |\mathbf{r}^0_{1\beta}| = |\mathbf{F}\mathbf{R}^0_{1\beta} + \boldsymbol{\xi}|, \quad \beta = 2,\ldots,5, \tag{25}$$

and

$$r^0_{\beta\gamma} = |\mathbf{r}^0_{\beta\gamma}| = |\mathbf{F}\mathbf{R}^0_{\beta\gamma}|, \quad \beta,\gamma = 2,\ldots,5; \quad \gamma\neq\beta. \tag{26}$$

Note that the inner displacements for atoms β and γ cancel out in Eq. (26) since the two atoms belong to the same Bravais lattice. From Eqs. (24)–(26), we note that $V_{1\beta}$ is a function of the atom positions in the initial configuration, the deformation gradient $\mathbf{F}$ and the inner displacement $\boldsymbol{\xi}$. The second Piola-Kirchhoff stress can then be rewritten as

$$\mathbf{S} = \frac{1}{2V_A}\frac{d}{d\mathbf{E}}\left(\sum_{\beta=2}^{5} V_{1\beta}\right) = \frac{1}{2V_A}\sum_{\beta=2}^{5}\left(\frac{\partial V_{1\beta}}{\partial \mathbf{E}} + \frac{\partial V_{1\beta}}{\partial \boldsymbol{\xi}}\frac{\partial \boldsymbol{\xi}}{\partial \mathbf{E}}\right). \tag{27}$$

For a given deformation gradient $\mathbf{F}$, the inner displacement $\boldsymbol{\xi}$ can be determined by minimizing the strain energy density function, i.e.,

$$\frac{1}{2V_A}\left(\sum_{\beta=2}^{5}\frac{\partial V_{1\beta}}{\partial \boldsymbol{\xi}}\right)_{\mathbf{F}} = 0. \tag{28}$$

Substituting Eq. (28) into Eq. (27), one obtains

$$\mathbf{S} = \frac{1}{2V_A}\sum_{\beta=2}^{5}\left(\frac{\partial V_{1\beta}}{\partial \mathbf{E}}\right) = \frac{\mathbf{F}^{-1}}{2V_A}\sum_{\beta=2}^{5}\left(\frac{\partial V_{1\beta}}{\partial \mathbf{F}}\right). \tag{29}$$

Substituting Eq. (24) into Eq. (29) and using the chain rule, the second Piola-Kirchhoff stress can be further rewritten as

$$\mathbf{S} = \frac{\mathbf{F}^{-1}}{2V_A}\sum_{\beta=2}^{5}\left[\frac{\partial V_{1\beta}}{\partial r^0_{1\beta}}\frac{\partial r^0_{1\beta}}{\partial \mathbf{F}} + \sum_{\substack{\gamma=2\\ \gamma\neq\beta}}^{5}\left(\frac{\partial V_{1\beta}}{\partial r^0_{1\gamma}}\frac{\partial r^0_{1\gamma}}{\partial \mathbf{F}} + \frac{\partial V_{1\beta}}{\partial \cos\theta^0_{1\beta\gamma}}\frac{\partial \cos\theta^0_{1\beta\gamma}}{\partial \mathbf{F}}\right)\right]. \tag{30}$$

The derivatives of the bond lengths $r^0_{1\beta}$, $r^0_{1\gamma}$ and the cosine of the bond angle $\cos\theta^0_{\alpha\beta\gamma}$, with respect to the deformation gradient $\mathbf{F}$ and the inner displacement $\boldsymbol{\xi}$, are given in Appendix A. The elastic constants can be computed from

$$\mathbf{C}_{ijkl} = \frac{\partial^2 W_U}{\partial \mathbf{E}_{ij}\partial \mathbf{E}_{kl}} - \frac{\partial^2 W_U}{\partial \mathbf{E}_{ij}\partial \boldsymbol{\xi}_m}\left(\frac{\partial^2 W_U}{\partial \boldsymbol{\xi}_m \partial \boldsymbol{\xi}_n}\right)^{-1}\frac{\partial^2 W_U}{\partial \boldsymbol{\xi}_n \partial \mathbf{E}_{kl}}, \quad i,j,k,l,m,n = 1,2,3, \tag{31}$$

where the first term on the right-hand side of Eq. (31) is the homogeneous part, which describes the elastic response when all the atoms are displaced homogeneously upon the application of the strain, and the second term on the right-hand side of Eq. (31) is the inhomogeneous part associated with the inner displacement $\boldsymbol{\xi}$ between the two fcc Bravais lattices under a uniform strain. As shown in Appendix B, Eq. (31) can be rewritten as

$$\mathbf{C}_{ijkl} = \mathbf{F}^{-1}_{in}\frac{\partial^2 W_U}{\partial \mathbf{F}_{nj}\partial \mathbf{F}_{mk}}\mathbf{F}^{-1}_{lm} - \mathbf{F}^{-1}_{in}\mathbf{F}^{-1}_{km}\frac{\partial W_U}{\partial \mathbf{F}_{mj}}\mathbf{F}^{-1}_{ln} - \mathbf{F}^{-1}_{ip}\frac{\partial^2 W_U}{\partial \mathbf{F}_{pj}\partial \boldsymbol{\xi}_m}\left(\frac{\partial^2 W_U}{\partial \boldsymbol{\xi}_m \partial \boldsymbol{\xi}_n}\right)^{-1}\mathbf{F}^{-1}_{kq}\frac{\partial^2 W_U}{\partial \mathbf{F}_{ql}\partial \boldsymbol{\xi}_n}, \quad i,j,k,l,m,n,p,q = 1,2,3, \tag{32}$$

where the elastic constants are expressed in terms of $\mathbf{F}$ and $\boldsymbol{\xi}$ and the derivatives of the strain energy density with respect to the deformation gradient $\mathbf{F}$ and the inner displacement $\boldsymbol{\xi}$ are obtained in a straightforward manner by using the results in Appendix A. After all the strain and stress tensors and their derivatives are calculated, the governing Eqs. (7)–(9) can be solved either by constructing a weak form (as is typically done in the finite element method) or by collocating the governing equations at the continuum nodes (as is typically done in a finite difference method or in a collocation meshless method[30]). We solve the governing equations using the collocation method, but the finite element method can also be implemented easily.

D. QC method at finite temperature

In the finite-temperature case, the silicon structure is considered as a thermodynamic system. For an isothermal system, the second Piola-Kirchhoff stress tensor at a constant temperature, T, is defined by[26]

$$\mathbf{S} = \left(\frac{dW_A}{d\mathbf{E}} \right)_T, \tag{33}$$

where the strain energy density function W in Eq. (10) is replaced by the Helmholtz free energy density function W_A. The Helmholtz free energy is calculated by using the theory of lattice dynamics with a quasiharmonic approximation of the interatomic potential. In a harmonic approximation, the Tersoff potential function is written in a quadratic form by neglecting the higher-order (>2) terms in its Taylor's series expansion. The total potential energy of a system of N atoms at any instantaneous position can thus be rewritten as

$$U(\boldsymbol{\eta}_1, \ldots, \boldsymbol{\eta}_N) = U(\boldsymbol{\eta}_1^0, \ldots, \boldsymbol{\eta}_N^0) + \frac{1}{2} \sum_{\beta,\gamma=1}^{N} \sum_{j,k=1}^{3} \left. \frac{\partial^2 U(\boldsymbol{\eta}_1, \ldots, \boldsymbol{\eta}_N)}{\partial \boldsymbol{\eta}_{\beta j} \partial \boldsymbol{\eta}_{\gamma k}} \right|_{\boldsymbol{\eta}_1, \ldots, \boldsymbol{\eta}_N = \boldsymbol{\eta}_1^0, \ldots, \boldsymbol{\eta}_N^0} \mathbf{v}_{\beta j} \mathbf{v}_{\gamma k}, \tag{34}$$

where $\boldsymbol{\eta}_{\beta j}$ and $\boldsymbol{\eta}_{\gamma k}$ are the jth and kth component of the relative position of atoms β and γ, respectively, and $\mathbf{v}_{\beta j}$ and $\mathbf{v}_{\gamma k}$ are the jth and kth component of the thermal vibrational displacement of atoms β and γ, respectively. Denoting $\boldsymbol{\eta} = (\boldsymbol{\eta}_1, \ldots, \boldsymbol{\eta}_N)$ and $\boldsymbol{\eta}^0 = (\boldsymbol{\eta}_1^0, \ldots, \boldsymbol{\eta}_N^0)$, Eq. (34) can be rewritten in a matrix form as

$$U(\boldsymbol{\eta}) = U(\boldsymbol{\eta}^0) + \tfrac{1}{2} \mathbf{v}^T \boldsymbol{\Phi} \mathbf{v}, \tag{35}$$

where $\mathbf{v} = (\mathbf{v}_1, \ldots, \mathbf{v}_N)^T$ and $\boldsymbol{\Phi}$ is the $3N \times 3N$ force constant matrix given by

$$\boldsymbol{\Phi}_{3\beta+j-3, 3\gamma+k-3} = \left. \frac{\partial^2 U(\boldsymbol{\eta})}{\partial \boldsymbol{\eta}_{\beta j} \partial \boldsymbol{\eta}_{\gamma k}} \right|_{\boldsymbol{\eta} = \boldsymbol{\eta}^0},$$

$$\beta, \gamma = 1, \ldots, N; \quad j, k = 1, 2, 3. \tag{36}$$

Note that $\boldsymbol{\eta}^0$ is a function of lattice constant a, the deformation gradient $\mathbf{F}$, and the inner displacement $\boldsymbol{\xi}$, as shown in Eqs. (4), (6), and (20)–(22). In a quasiharmonic approximation, the lattice constant is a function of temperature. For a crystal lattice, the normal vibrational frequencies can be computed from the force constant matrix by using the theory of lattice dynamics. Once the vibrational frequencies are obtained, the Helmholtz free energy A can be readily computed as[25]

$$A = U^0 + \frac{1}{2} \sum_n \hbar \, \omega_n + k_B T \sum_n \ln(1 - e^{-\hbar \omega_n / k_B T}), \tag{37}$$

where $U^0 \equiv U(\boldsymbol{\eta}^0)$ denotes the total potential energy evaluated at the equilibrium position of the system, $\hbar$ is the reduced Planck's constant, k_B is the Boltzmann constant, and ω_n is the vibrational frequency of the nth normal mode of the crystal lattice. Note that on the right-hand side of Eq. (37), the first term is the static potential energy, the second term is the quantum-mechanical zero point energy and the sum of the second and the third terms is the vibrational Helmholtz free energy. The Helmholtz free energy density for an atom α is given by

$$W_A = \frac{1}{V_A} \left(U_\alpha^0 + \frac{1}{N} \sum_n \left[\frac{1}{2} \hbar \, \omega_n + k_B T \ln(1 - e^{-\hbar \omega_n / k_B T}) \right] \right), \tag{38}$$

where V_A is the volume of atom α in the initial configuration, and $U_\alpha^0 \equiv U_\alpha(\boldsymbol{\eta}^0)$ denotes the potential energy of atom α evaluated using the equilibrium position of the system. Note that $U^0 = \Sigma_{\alpha=1}^N U_\alpha^0$.

In the quasiharmonic approximation, the elements of the force constant matrix given in Eq. (36) are a function of the lattice constant a, the deformation gradient $\mathbf{F}$, and the inner displacement $\boldsymbol{\xi}$. Therefore, the vibrational frequencies, ω_n, and the Helmholtz free energy density function, W_A, are also functions of a, $\mathbf{F}$, and $\boldsymbol{\xi}$. For a given temperature T the lattice constant a is first determined on the unstrained silicon crystal by

$$\left(\frac{\partial A}{\partial a} \right)_T = 0. \tag{39}$$

More details on the determination of the lattice constant can be found in Ref. 29. As discussed in Sec. II C, the inner displacement $\boldsymbol{\xi}$ can be determined by minimizing W_A for a given deformation gradient $\mathbf{F}$, i.e.,

$$\left(\frac{\partial W_A}{\partial \boldsymbol{\xi}} \right)_{\mathbf{F}} = 0. \tag{40}$$

After $\boldsymbol{\xi}$ is determined, the second Piola-Kirchhoff stress is then calculated as

$$\mathbf{S} = \left(\frac{\partial W_A}{\partial \mathbf{E}} + \frac{\partial W_A}{\partial \boldsymbol{\xi}} \frac{\partial \boldsymbol{\xi}}{\partial \mathbf{E}} \right) = \frac{\partial W_A}{\partial \mathbf{E}} = \mathbf{F}^{-1} \frac{\partial W_A}{\partial \mathbf{F}}. \tag{41}$$

Substituting Eq. (38) into Eq. (41), we have

$$\mathbf{S} = \frac{\mathbf{F}^{-1}}{V_A} \left[\frac{\partial U_\alpha^0}{\partial \mathbf{F}} + \frac{\hbar}{N} \sum_n \left(\frac{1}{2} + \frac{1}{e^{\hbar \omega_n / k_B T} - 1} \right) \frac{\partial \omega_n}{\partial \mathbf{F}} \right]. \tag{42}$$

By defining the generalized phonon Grüneisen parameter (GPGP),[26]

$$\gamma^{(n)}(\mathbf{F}) = -\mathbf{F}^{-1} \frac{d \ln \omega_n}{d\mathbf{F}}, \tag{43}$$

$\mathbf{S}$ can also be rewritten as

$$\mathbf{S} = \frac{1}{V_A} \left[\mathbf{F}^{-1} \frac{\partial U_\alpha^0}{\partial \mathbf{F}} - \frac{\hbar}{N} \sum_n \left(\frac{1}{2} + \frac{1}{e^{\hbar \omega_n / k_B T} - 1} \right) \omega_n \gamma^{(n)} \right]. \tag{44}$$

The isothermal elastic constants are now given by (see Appendix B),

$$\mathbf{C}_{ijkl} = \mathbf{F}^{-1}_{in}\frac{\partial^2 W_A}{\partial \mathbf{F}_{nj}\,\partial \mathbf{F}_{mk}}\mathbf{F}^{-1}_{lm} - \mathbf{F}^{-1}_{in}\mathbf{F}^{-1}_{km}\frac{\partial W_A}{\partial \mathbf{F}_{mj}}\mathbf{F}^{-1}_{ln} - \mathbf{F}^{-1}_{ip}\frac{\partial^2 W_A}{\partial \mathbf{F}_{pj}\,\partial \boldsymbol{\xi}_m}\left(\frac{\partial^2 W_A}{\partial \boldsymbol{\xi}_m\,\partial \boldsymbol{\xi}_n}\right)^{-1}\mathbf{F}^{-1}_{kq}\frac{\partial^2 W_A}{\partial \mathbf{F}_{ql}\,\partial \boldsymbol{\xi}_n},$$

$$i,j,k,l,m,n,p,q = 1,2,3. \tag{45}$$

The procedure for computing the derivatives of the vibrational frequencies with respect to the deformation gradient and the inner displacement, i.e., $\partial\omega_n/\partial\mathbf{F}$ and $\partial\omega_n/\partial\boldsymbol{\xi}$, is given in Appendix C. Once the isothermal elastic constants are obtained, the adiabatic elastic constants $\bar{\mathbf{C}}_{ijkl}$ can be computed by[26]

$$\bar{\mathbf{C}}_{ijkl} = \mathbf{C}_{ijkl} - \left(\frac{\partial^2 W_A}{\partial T^2}\right)^{-1}\frac{\partial^2 W_A}{\partial T\,\partial \mathbf{E}_{ij}}\frac{\partial^2 W_A}{\partial T\,\partial \mathbf{E}_{kl}}. \tag{46}$$

In the general procedure illustrated in Eqs. (33)–(46), a key step is to calculate the vibrational frequencies ω_n from the force constant matrix. Several quasiharmonic models can be used to calculate the vibrational frequencies,[29] including the QHM model,[25] the LQHM model,[22] and the QHMK model.[31] In the following sections, we describe how the vibrational frequencies are obtained with each of the models and provide expressions for the second Piola-Kirchhoff stress and other quantities that are specific to each model.

1. Real space quasiharmonic (QHM) model

In the QHM model, the vibrational frequencies are given by $\omega_j = \sqrt{\lambda_j/M}$, where M is the mass of the silicon atom, and λ_j $(j=1,2,\ldots,3N)$ are the eigenvalues computed from the $3N\times 3N$ force constant matrix $\mathbf{\Phi}$ which is defined in Eq. (36). The Helmholtz free energy for an N-atom crystal lattice is given by[26]

$$A = \sum_{\alpha=1}^{N} U^0_\alpha + \frac{1}{2}\sum_{j=1}^{3N}\hbar\,\omega_j + k_B T\sum_{j=1}^{3N}\ln(1-e^{-\hbar\omega_j/k_B T}). \tag{47}$$

The Helmholtz free energy density for an atom α is given by

$$W_A = \frac{1}{V_A}\left[U^0_\alpha + \frac{1}{N}\sum_{j=1}^{3N}\left(\frac{\hbar\,\omega_j}{2} + k_B T\ln(1-e^{-\hbar\omega_j/k_B T})\right)\right]. \tag{48}$$

The second Piola-Kirchhoff stress is calculated from Eq. (42) as

$$\mathbf{S} = \frac{\mathbf{F}^{-1}}{V_A}\left[\frac{\partial U^0_\alpha}{\partial \mathbf{F}} + \frac{\hbar}{N}\sum_{j=1}^{3N}\left(\frac{1}{2} + \frac{1}{e^{\hbar\omega_j/k_B T}-1}\right)\frac{\partial\omega_j}{\partial \mathbf{F}}\right]. \tag{49}$$

The elastic constants can be calculated by using Eqs. (45) and (46).

The QHM model directly computes all the normal modes and the vibrational frequencies of the system. While the surface effects and/or defects in a nanostructure can be readily captured in the QHM model, the number of atoms that can be considered in this approach is limited due to the fact that the eigenvalues and their derivatives of a $3N\times 3N$ system must be computed. Typically, the number of atoms N that can be considered is of the order of several hundreds. For nanostructures with a characteristic length larger than a few nanometers the QHM approach described by Eqs. (48) and (49) can be inefficient.

2. Local quasiharmonic (LQHM) model

The LQHM model has been proposed as a simple and a reasonably accurate model to compute the Helmholtz free energy of solid systems.[22] In the local quasiharmonic approximation, the coupling between the vibrations of different atoms is neglected and the atoms of the system are considered as independent harmonic oscillators. In other words, for a homogeneous system such as a perfect crystal lattice, all the atoms have the same vibrational frequencies. The force constant matrix [Eq. (36)] can be decomposed into N 3×3 local force constant matrices. The 3×3 local force constant matrix $\mathbf{\Phi}(\alpha)$ for an atom α is given by

$$\mathbf{\Phi}_{j,k}(\alpha) = \left.\frac{\partial^2 U_{\text{local}}(\alpha)}{\partial\boldsymbol{\eta}_{\alpha j}\,\partial\boldsymbol{\eta}_{\alpha k}}\right|_{\boldsymbol{\eta}=\boldsymbol{\eta}^0}, \quad j,k=1,2,3, \tag{50}$$

where $U_{\text{local}}(\alpha)$ is the local potential energy of atom α, which contains contributions from the first and the second nearest neighbors of center atom α. In the LQHM model, the center atom α vibrates about its equilibrium position while the surrounding atoms are considered fixed. As shown by the 17-atom cluster in Fig. 1, the instantaneous position of the center atom $(\alpha=1)$ affects the potential energy of atoms 1–5, i.e., the potential energy U_β, $\beta=1,\ldots,5$, is a function of the center atom position. Therefore, $U_{\text{local}}(\alpha)$ can be calculated within a cell that includes the first and the second nearest neighbors of the center atom (i.e., 17 atoms as shown in Fig. 1). $U_{\text{local}}(\alpha)$ is given by

$$U_{\text{local}}(\alpha) = \sum_{\beta=1}^{5} U_\beta(\boldsymbol{\eta}_\sigma), \quad \alpha=1;\sigma\in\{1,\ldots,17\}, \tag{51}$$

where $\boldsymbol{\eta}_\sigma$ (σ takes values of β and its neighbors) denotes the position of atom β and its four neighbor atoms, and U_β is the potential energy of atom β. By diagonalizing the local force constant matrix $\mathbf{\Phi}(\alpha)$, the three vibrational frequencies $\omega_{\alpha j}$ can be determined, i.e., $\omega_{\alpha j} = \sqrt{\lambda_{\alpha j}/M}$, where $\lambda_{\alpha j}$ $(j=1,2,3)$ are the eigenvalues of the 3×3 force constant matrix $\mathbf{\Phi}(\alpha)$. The Helmholtz free energy for an atom α is given by[22]

$$A(\alpha) = U^0_\alpha + \frac{1}{2}\sum_{j=1}^{3}\hbar\,\omega_{\alpha j} + k_B T\sum_{j=1}^{3}\ln\left(1-e^{-\hbar\omega_{\alpha j}/k_B T}\right). \tag{52}$$

The Helmholtz free energy for an N-atom crystal lattice is given by $A=\sum_{\alpha=1}^{N}A(\alpha)$. The Helmholtz free energy density function for an atom α is then given by $W_A=A(\alpha)/V_A$, and the second Piola-Kirchhoff stress for an atom α is given by

$$\mathbf{S} = \frac{\mathbf{F}^{-1}}{V_A}\left[\frac{\partial U_\alpha^0}{\partial \mathbf{F}} + \hbar \sum_{j=1}^{3}\left(\frac{1}{2} + \frac{1}{e^{\hbar\omega_{\alpha j}/k_B T} - 1}\right)\frac{\partial \omega_{\alpha j}}{\partial \mathbf{F}}\right]. \quad (53)$$

The elastic constants can again be computed by using Eqs. (45) and (46).

The LQHM model is computationally attractive, as it reduces the degrees of freedom by neglecting the correlations between the vibrations of different atoms, and has been used[18–21] to extend the QC method at classical 0 K to finite temperature cases. As shown in Ref. 29 and as pointed out in Sec. IV B, the LQHM model can be inaccurate in describing the thermal and elastic properties as it neglects the vibrational coupling of the atoms. For this reason, nonlocal quasiharmonic models are necessary to accurately calculate the material properties.

3. k-space quasiharmonic (QHMK) model

For a perfect crystal lattice with homogeneous deformation, the Helmholtz free energy can be computed efficiently in the reciprocal space by using the Bloch's theorem[32] with the Born–von Karman boundary condition. In the reciprocal representation, the force constant matrix defined by Eq. (36) can be reduced to a 6×6 dynamical matrix by using Fourier transformation as (see Ref. 29 for details)

$$\mathbf{D}(\mathbf{k}) = \frac{1}{M}\begin{bmatrix} \sum_{\beta=1}^{N} \mathbf{\Phi}_{j,k}^{11}(\alpha,\beta) e^{i\mathbf{k}\cdot\mathbf{R}_{\beta\alpha}^0} & \sum_{\beta=1}^{N} \mathbf{\Phi}_{j,k}^{12}(\alpha,\beta) e^{i\mathbf{k}\cdot(\mathbf{R}_{\beta\alpha}^0 - \mathbf{F}^{-1}\boldsymbol{\xi})} \\ \sum_{\beta=1}^{N} \mathbf{\Phi}_{j,k}^{21}(\alpha,\beta) e^{i\mathbf{k}\cdot(\mathbf{R}_{\beta\alpha}^0 + \mathbf{F}^{-1}\boldsymbol{\xi})} & \sum_{\beta=1}^{N} \mathbf{\Phi}_{j,k}^{22}(\alpha,\beta) e^{i\mathbf{k}\cdot\mathbf{R}_{\beta\alpha}^0} \end{bmatrix}, \quad \alpha = 1; \quad j,k = 1,2,3, \quad (54)$$

where $\mathbf{k}$ is the wave vector and, for a given N atom silicon lattice, $N/2$ $\mathbf{k}$ points can be chosen to lie in the first Brillouin zone (FBZ) due to the periodicity of the reciprocal lattice,[31] and $\mathbf{\Phi}_{j,k}^{pq}(\alpha,\beta)$ is given by

$$\mathbf{\Phi}_{j,k}^{pq}(\alpha,\beta) = \left.\frac{\partial^2 U(\boldsymbol{\eta})}{\partial \boldsymbol{\eta}_{\alpha j}\, \partial \boldsymbol{\eta}_{\beta k}}\right|_{\boldsymbol{\eta}=\boldsymbol{\eta}^0(\mathbf{F},\boldsymbol{\xi}),\alpha\in B_p,\beta\in B_q},$$

$$\alpha = 1; \quad \beta = 1,\ldots,N; \quad p,q = 1,2; \quad j,k = 1,2,3. \quad (55)$$

In the above equations, α is the center atom selected to compute the dynamical matrix, and B_p and B_q denote the pth and the qth Bravais lattices, respectively. In the calculation of the dynamical matrix, for the center atom α, atom β loops over all the atoms in the crystal lattice. However, as the Tersoff potential only includes the nearest neighbor interactions, it can be shown that $\mathbf{\Phi}_{j,k}^{pq}(\alpha,\beta)$ has nonzero values only if the atom β is within two layers of atoms surrounding the center atom α. Therefore, the force constant matrix can be obtained by the calculation within a cell that includes the second nearest neighbors (total 17 atoms for diamond structure crystal silicon) of a center atom α, as shown by the 17-atom cluster in Fig. 1. More details on the calculation of the dynamical matrix for Tersoff silicon can be found in Ref. 29.

The vibrational frequencies can be calculated by $\omega_s(\mathbf{k}) = \sqrt{\lambda_s(\mathbf{k})}$, where $\lambda_s(\mathbf{k})$ are the eigenvalues of the 6×6 dynamical matrix $\mathbf{D}$ and s is the index of the polarization for silicon crystal. In the reciprocal representation, the Helmholtz free energy for an N-atom crystal lattice is given by[29,31]

$$A = U^0 + \frac{1}{2}\sum_{\mathbf{k}}\sum_{s=1}^{6} \hbar\,\omega_s(\mathbf{k}) + k_B T \sum_{\mathbf{k}}\sum_{s=1}^{6} \ln(1 - e^{-\hbar\omega_s(\mathbf{k})/k_B T}). \quad (56)$$

For a bulk silicon crystal, $\mathbf{k}$ can be taken as a continuous variable and $\Sigma_{\mathbf{k}}$ in Eq. (56) can be replaced by an integral. Therefore, the Helmholtz free energy density for an atom α is given by

$$W_A = \frac{U_\alpha^0}{V_A} + \frac{1}{2V_A V_B}\left(\frac{1}{2}\int_{\mathbf{k}}\sum_{s=1}^{6} \hbar\,\omega_s(\mathbf{k})\,d\mathbf{k} + k_B T \int_{\mathbf{k}}\sum_{s=1}^{6} \ln(1 - e^{-\hbar\omega_s(\mathbf{k})/k_B T})\,d\mathbf{k}\right), \quad (57)$$

where V_B is the volume of the first Brillouin zone of the reciprocal lattice and the factor 2 is due to the two Bravais lattices of a silicon crystal. The first term and the second term on the right-hand side of Eq. (57) are the static and the vibrational component of the Helmholtz free energy density, respectively. After the Helmholtz free energy density is obtained, the second Piola-Kirchhoff stress is given by

$$\mathbf{S} = \frac{\mathbf{F}^{-1}}{V_A}\left[\frac{\partial U_\alpha^0}{\partial \mathbf{F}} + \frac{\hbar}{2V_B}\sum_{s=1}^{6}\int_{\mathbf{k}}\left(\frac{1}{2} + \frac{1}{e^{\hbar\omega_s(\mathbf{k})/k_B T} - 1}\right)\frac{\partial \omega_s(\mathbf{k})}{\partial \mathbf{F}}\,d\mathbf{k}\right]. \quad (58)$$

The elastic constants can again be obtained by using Eqs. (45) and (46).

The QHMK model is mathematically equivalent to the QHM model with the Born–von Karman boundary condition (see Ref. 29 for more details). In the QHMK model, the vibrational component of the Helmholtz free energy density [the second term on the right-hand side of Eq. (57)] for the atom corresponding to the continuum node, $\mathbf{X}$, is computed by using a bulk (*nonlocal*) silicon crystal lattice. The *nonlocal* silicon crystal lattice is, however, assumed to be sub-

jected to a homogeneous deformation given by the *local* deformation gradient $\mathbf{F}(\mathbf{X})$. We refer to this approximation as the "semilocal" approximation to compute the vibrational free energy density. For large crystal structures where the surface effects are negligible and each continuum node represents a large number of atoms, the semilocal approximation can be an accurate and an efficient way to compute the vibrational Helmholtz free energy of the structure.[29]

III. MOLECULAR DYNAMICS SIMULATION OF SILICON NANOSTRUCTURES

We developed a molecular dynamics code to simulate the mechanical behavior of nanostructures with applied external loads. In the MD simulations, the atoms of the nanostructure are initially positioned at the ideal diamond lattice sites, and then relaxed to the equilibrium position after the external loads are applied. In the initialization step, the velocities are randomized to satisfy the Maxwell-Boltzmann distribution at the prescribed temperature. For the MD simulation results presented in this paper, the relaxation step was performed for 2 ns with a time step of 0.2 fs. Once the equilibrium state is reached, about 10 000 more time steps are performed for time averaging purpose. The temperature is controlled by using a Nosé-Hoover thermostat.[33] The Newtonian equations of motion are integrated by the standard Verlet leapfrog algorithm. Verlet's neighbor lists are also employed to improve the performance of the code.[34] The bonded interactions for the silicon material are modeled by using the Tersoff potential.

Since MD simulations obey the rules of classical statistical mechanics, quantum corrections are necessary when the results are compared with quantum-mechanical calculations or experiments, especially at low temperatures. We implemented the temperature scaling method proposed in Ref. 35. In this method the scaled MD temperature, T_{MD}, (corresponding to a real temperature T) is computed by requiring that the internal energy of the classical system be identical to that of the corresponding quantum system at T. This leads to the scaling relation

$$T_{MD} = \frac{1}{3(N-1)k_B} \sum_{\mathbf{k}} \sum_{s=1}^{6} \hbar\, \omega_s(\mathbf{k}) \left(\frac{1}{2} + \frac{1}{e^{\hbar \omega_s(\mathbf{k})/k_B T} - 1} \right), \tag{59}$$

where N is the total number of atoms in the system. Note that, since the QHMK model describes the thermal properties of the bulk silicon crystal lattice more accurately,[29] we adopt the QHMK model for the quantum correction of the temperature.

The molecular dynamics code is used to perform stretch and bending tests on silicon structures. For a stretch test on a silicon nanostructure, the center atom in the left surface layer is fixed along all the three Cartesian directions to prevent translational movement of the structure. All the other atoms at the left end of the structure are fixed along the x direction and are allowed to move freely along the y and z directions, i.e., the nanostructure can expand or contract freely along the y and z directions. The external loads are applied on the atoms in the right surface layer. For bending tests on silicon nanostructures, the appropriate layer of atoms at the end(s) of the nanostructures are fixed along all the three Cartesian directions.

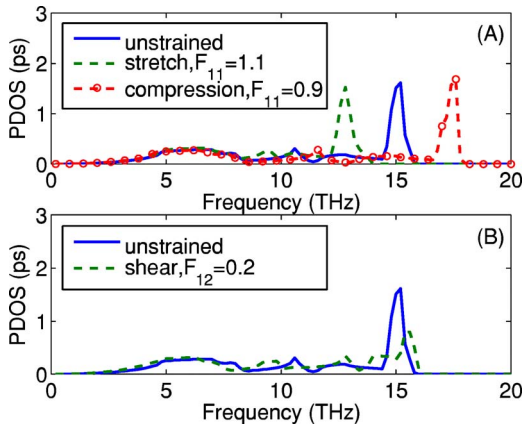

FIG. 2. (Color online) (a) PDOS for stretch and compression conditions; (b) PDOS under a shear condition. $T=1000$ K.

IV. RESULTS AND DISCUSSION

A. Strain and temperature effects on PDOS and Grüneisen parameters

The PDOS represents the number of vibrational modes per unit phonon frequency per atom. In this paper, for the calculation of PDOS, we adopt the direct sampling method, which generates a large number of uniformly distributed $\mathbf{k}$ points in the FBZ and approximates the PDOS by a normalized histogram.[36] In our calculation, $100\times100\times100/2$ points uniformly distributed in the first quadrant of the FBZ are used. To investigate the strain effect on the PDOS at finite temperature, the lattice constant is first determined by solving Eq. (39). Next for a given deformation gradient $\mathbf{F}$, the inner displacement $\boldsymbol{\xi}$ is determined by solving Eq. (40). The phonon frequencies can then be obtained from the eigenvalues of the dynamical matrix. The effect of strain on the PDOS at $T=1000$ K is shown in Fig. 2. We observe that when a uniaxial deformation is applied, a shift of optical phonons and splitting of their degeneracies occur, while the acoustic phonons do not vary much, as shown in Fig. 2(a). Figure 2(b) shows that a shear deformation primarily causes a splitting of the degeneracies, especially for the optical phonons.

The GPGPs $\gamma_{ij}^{(n)}$ defined by Eq. (43) measure the variation of the phonon frequency ω_n with deformation at a constant temperature. These parameters can be used directly in the calculation of the stress tensor as shown in Eq. (44). The volumetric phonon Grüneisen parameter (PGP) for unstrained silicon crystal, which is defined as $\gamma_V^{(n)} = -d(\ln \omega_n)/d(\ln V)$, where V is the lattice volume, can be calculated from the GPGPs by $\gamma_V^{(n)} = (\gamma_{11}^{(n)} + \gamma_{22}^{(n)} + \gamma_{33}^{(n)})/3$. The volumetric PGP for unstrained Tersoff silicon at 0 K (classical) has already been calculated in Ref. 37. In this paper, we investigate the temperature effect on the PGP for unstrained Tersoff silicon at finite temperature. First, the lattice constant

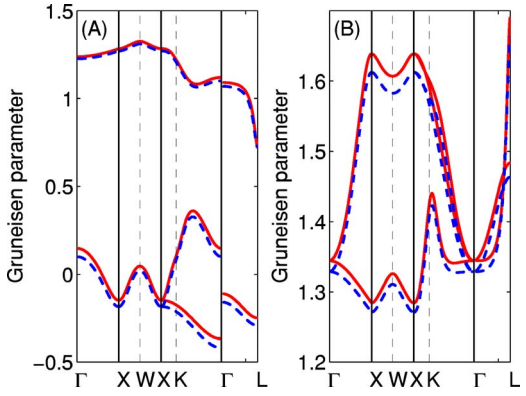

FIG. 3. (Color online) The volumetric PGP γ_V for unstrained Tersoff silicon: (a) The acoustic modes at 0 K (the dashed lines) and 1000 K (the solid line); (b) the optical modes at 0 K (the dashed lines) and 1000 K (the solid lines).

is determined by using Eq. (39). In the QHMK method, the phonon dispersion relations $\omega=\omega_s(\mathbf{k})$ are obtained by numerically diagonalizing Eq. (54) for different wave vectors $\mathbf{k}$, which are usually chosen along several special directions in the FBZ. By differentiating the phonon dispersion relations with respect to the deformation gradient $\mathbf{F}$, the GPGPs as a function of the wave vector $\mathbf{k}$ are obtained by using $\gamma_{ij}^{(\mathbf{k}s)}=-\mathbf{F}_{im}^{-1}d[\ln\omega_s(\mathbf{k},\mathbf{F})]/d\mathbf{F}_{mj}$, $i,j,m=1,2,3$. The volumetric PGPs γ_V obtained from the QHMK method at two different temperatures are shown in Fig. 3. We observe that the Grüneisen parameters for both the acoustic modes and the optical modes increase as the temperature increases and the shifts are due to the thermal expansion. In the LQHM method, the three phonon frequencies degenerate into one value for the unstrained silicon, and the volumetric PGPs are calculated as 1.295 at $T=0$ K and 1.317 at $T=1000$ K.

B. Bulk elastic constants

The elastic constants are the key parameters in the constitutive laws describing a material. We have determined the isothermal and adiabatic elastic constants of Tersoff silicon for several cases.

First, when quantum-mechanical effects are neglected at 0 K, i.e., when the zero point energy [the second term on the right-hand side of Eq. (56)] is neglected, the characteristic energy is the lattice potential energy. In this case, the elastic constants are simply the second derivatives of the potential energy density function with respect to the strain and the inner displacement as given by Eq. (31). Since the unstrained silicon crystal lattice is cubic symmetric,[38] the pairs ij and kl in $\mathbf{C}_{ijkl}$ can be replaced by a single index p in the Voigt notation: $ij=11\rightarrow p=1$, $ij=22\rightarrow p=2$, and $ij=12$ or $21\rightarrow p=4$. For example, $\mathbf{C}_{1212}$ is replaced by $\mathbf{C}_{44}$. The elastic constants computed at classical 0 K for the second Tersoff (T2) model[39] are, $C_{11}=1.218$ Mbars, $C_{12}=0.859$ Mbar, $C_{44}=0.103$ Mbar, and $C_{44}^0=0.924$ Mbar, where C_{44}^0 is C_{44} computed by neglecting the inner displacement $\boldsymbol{\xi}$. For the third Tersoff (T3) model,[23] $C_{11}=1.428$ Mbars, $C_{12}=0.756$ Mbar, $C_{44}=0.690$ Mbar, and $C_{44}^0=1.189$ Mbars. These results match the calculations performed in Ref. 28. The Cauchy discrepancy, which is defined as $(C_{12}-C_{44})$, for the T2 model is 0.756 Mbar, for the T3 model is 0.066 Mbar, and from experiments is −0.16 Mbar.

Second, the adiabatic elastic constants at finite temperature and zero strain are calculated by using the QHMK, LQHM, and the QHM models. We first calculate the isothermal elastic constants and the adiabatic elastic constants are then obtained by using Eq. (46). We use 4000 $\mathbf{k}$ points for the QHMK calculations. For various temperatures, the calculated elastic constants and the comparison with published data are summarized in Table I. In the calculations using the QHM model, $5\times5\times5$ unit cells (1000 atoms) with periodic boundary conditions are used. We observe that the results from the QHMK model match well with those from atomistic simulations over a large temperature range while those from the LQHM model deviate from atomistic simulations (especially the results for $\mathbf{C}_{12}$). The QHM model results are identical to the results obtained from the QHMK model with $1000/2=500$ $\mathbf{k}$ points. The maximum deviation between the QHM model results with 1000 atoms and the QHMK model results with 4000 $\mathbf{k}$ points (shown in Table I) is less than 5×10^{-4} Mbar. However, the computational cost of the QHM model is several orders of magnitude higher that of the QHMK model. For this reason, the QHM model is not used for the rest of the calculations shown in this paper.

Third, we investigated the strain effect on the isothermal elastic constants at both 0 and 1000 K. Both QHMK and LQHM models are employed to calculate the elastic constants. In Fig. 4, the component $\mathbf{F}_{11}$ of the deformation gradient is varied from 0.85 to 1.15 to investigate the effect of compression ($\mathbf{F}_{11}<1$) and tension ($\mathbf{F}_{11}>1$) along the x direction. The elastic constants decrease as the material is stretched and increase as the material is compressed. Note that the cubic symmetry of the unstrained silicon crystal lattice breaks down due to the strain effect and this results in $\mathbf{C}_{1111}\neq\mathbf{C}_{2222}$, as shown in Fig. 4. Figure 5 shows the variation of the elastic constants with $\mathbf{F}_{12}$, which represents a shear deformation along the y direction. In this case, due to the introduction of shear strain, the elastic constants corresponding to the shear strain and stress relationships become nonzero, i.e., $\mathbf{C}_{1112},\mathbf{C}_{2212}\neq0$. Since $\mathbf{E}_{12}=\mathbf{E}_{21}$ under any deformation, the following symmetric properties remain: $\mathbf{C}_{1112}=\mathbf{C}_{1121}$, $\mathbf{C}_{2212}=\mathbf{C}_{2221}$, and $\mathbf{C}_{1212}=\mathbf{C}_{1221}=\mathbf{C}_{2112}=\mathbf{C}_{2121}$. As shown in Figs. 4 and 5, the LQHM model results can deviate by as much as 15% compared to the QHMK model results at 1000 K. The LQHM model results can deviate significantly (>30%) when the silicon crystal is under a general strain condition at 1000 K as shown in Fig. 6. From these results, we can conclude that the elastic constants from the LQHM model can be inaccurate for Tersoff silicon, especially when the material is under strain at high temperature.

C. Mechanical behavior of nanostructures under external loads

In Sec. II, we have described the multiscale QC approach for zero and finite-temperature conditions. In this section, we employ the multiscale QC approach to perform a mechanical

TABLE I. Adiabatic elastic constants (in Mbars) for Tersoff silicon at various temperatures.

	QHMK			LQHM			QHM			Atomistic simulations		
T (K)	C_{11}	C_{12}	C_{44}	C_{11}	C_{12}	C_{44}	C_{11}	C_{12}	C_{44}	C_{11}	C_{12}	C_{44}
100	1.392	0.740	0.672	1.392	0.738	0.673						
180.7	1.386	0.738	0.669	1.387	0.734	0.671	1.386	0.738	0.669	1.388[a]	0.742[a]	0.673 ±0.138[a]
300	1.372	0.732	0.662	1.373	0.725	0.667						
500	1.345	0.719	0.648	1.346	0.708	0.656	1.345	0.719	0.648			
700	1.315	0.706	0.633	1.317	0.691	0.644						
844.6	1.293	0.696	0.622	1.295	0.678	0.635	1.293	0.696	0.622	1.307 ±0.002[b]	0.708 ±0.002 [b]	0.620 ±0.01[b]
900	1.285	0.692	0.618	1.287	0.673	0.631						
1000	1.270	0.685	0.611	1.272	0.664	0.625	1.270	0.685	0.611			
1100	1.255	0.678	0.603	1.256	0.655	0.618						
1300	1.225	0.663	0.588	1.225	0.636	0.605						
1460.6	1.200	0.652	0.575	1.200	0.621	0.594	1.200	0.652	0.575	1.228[a]	0.681[a]	0.592 ±0.01[a]
1500	1.194	0.649	0.572	1.194	0.617	0.591						

[a]Data from Ref. 40.
[b]Data from Ref. 41.

analysis of silicon nanostructures under external loads at zero and finite temperatures. Both the LQHM and the QHMK models are employed in all the calculations for finite temperature, and all the calculations for 0 K are carried out with quantum-mechanical effects included, i.e., the zero point energy is calculated as shown in Eq. (52) for the LQHM model and Eq. (56) for the QHMK model. Shown in Fig. 7 are results for both compression and stretch tests on a silicon beam with a geometry of 10(length)×20(width)×10(thickness) unit cells, i.e., $5.432\times10.864\times5.432$ nm^3 (17 037 atoms in MD simulations) at 0 and 1000 K. The MD results are also presented in Fig. 7 for comparison. The temperature in MD is scaled by using Eq. (59). The results in Fig. 7 show the significance of temperature on the displacement of the structure. In addition, we observe that in the compression region (pressure<0) the LQHM model underestimates the displacement of the structure, due to its overestimation of the elastic constants when the crystal structure is under compression (see Fig. 4); while in the tensile region the results from the LQHM model are close to the QHMK model results, since both models give similar elastic constants under tension. The temperature effect is captured by the finite-temperature QC approach and the accuracy of the method is verified by the MD results. Figures 8 and 9 show bending tests at 0 and 1000 K on a silicon beam with a geometry of $40\times20\times10$ unit cells, i.e., $21.728\times10.864\times5.432$ nm^3 (66 867 atoms in MD simulations), with fixed-fixed and cantilever boundary conditions, respectively. When

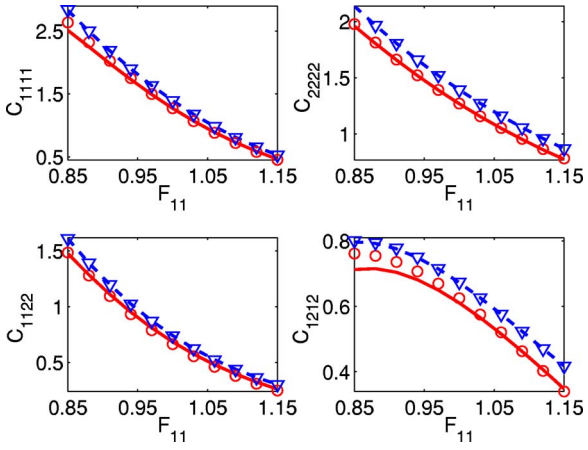

FIG. 4. (Color online) Elastic constants (in Mbars) when the lattice is under compression ($\mathbf{F}_{11}<1$) and tension ($\mathbf{F}_{11}>1$). The dashed lines are the QHMK results for $T=0$ K, the triangles are the LQHM results for $T=0$ K, the solid lines are the QHMK results for $T=1000$ K, and the circles are the LQHM results for $T=1000$ K.

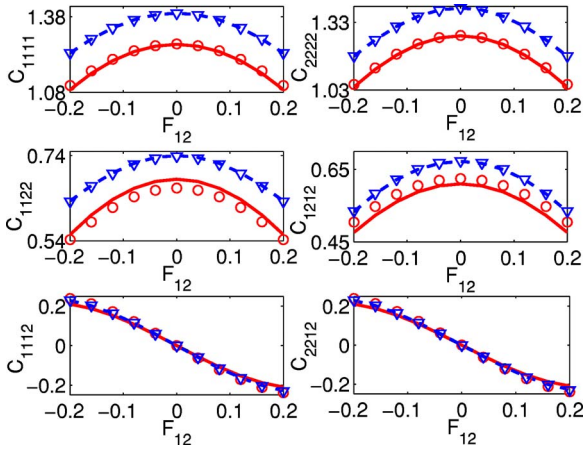

FIG. 5. (Color online) Elastic constants (in Mbars) as a function of shear deformation. The dashed lines are the QHMK results for $T=0$ K, the triangles are the LQHM results for $T=0$ K, the solid lines are the QHMK results for $T=1000$ K, and the circles are the LQHM results for $T=1000$ K.

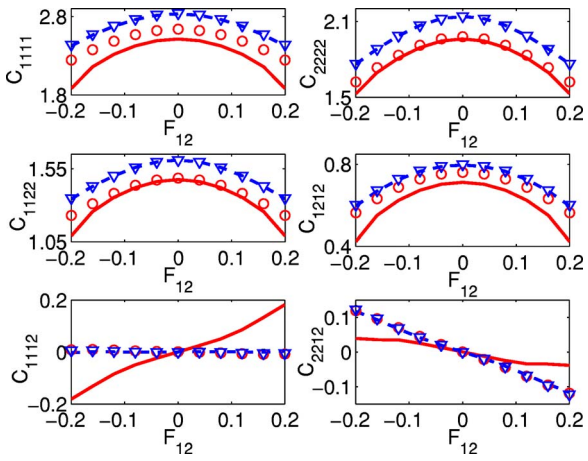

FIG. 6. (Color online) Elastic constants (in Mbars) at 1000 K under a combined deformation of $\mathbf{F}_{11}=0.85$ and $\mathbf{F}_{12}$ varies from −0.2 to 0.2. The dashed lines are the QHMK results for $T=0$ K, the triangles are the LQHM results for $T=0$ K, the solid lines are the QHMK results for $T=1000$ K, and the circles are the LQHM results for $T=1000$ K.

the temperature is high (1000 K in this case) the results from the QC method start to deviate from the MD results due to the anharmonic effects of the interatomic potential. Figure 10 shows results for a silicon beam with a geometry of $10\times20\times10$ unit cells, i.e., $5.432\times10.864\times5.432$ nm^3 (17 037 atoms in MD simulations), subjected to a general loading condition. The deformation of the beam resembles the deformation condition under which the elastic constants shown in Fig. 6 are computed. In this case, the results obtained from the QHMK model agree well with the MD results, while the LQHM results are in significant error compared to the MD results. The error can be explained by the elastic constants shown in Fig. 6, where most of the elastic constants predicted by the LQHM model are significantly higher than those computed by using the QHMK model.

When the characteristic length of the nanostructure is large, the surface effects, which arise due to the different

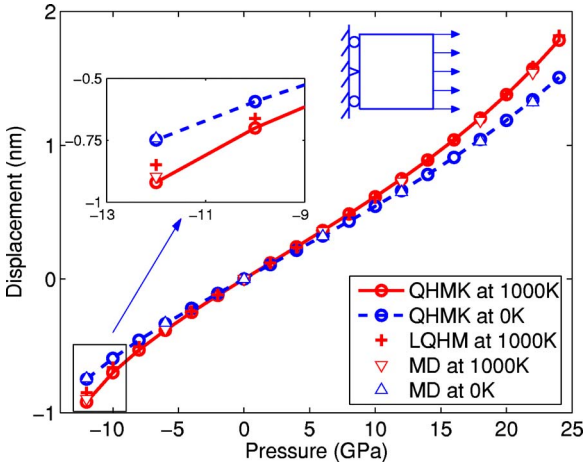

FIG. 7. (Color online) The peak displacement as a function of the applied compression pressure (<0) and tensile pressure (>0) for a silicon beam at 0 and 1000 K.

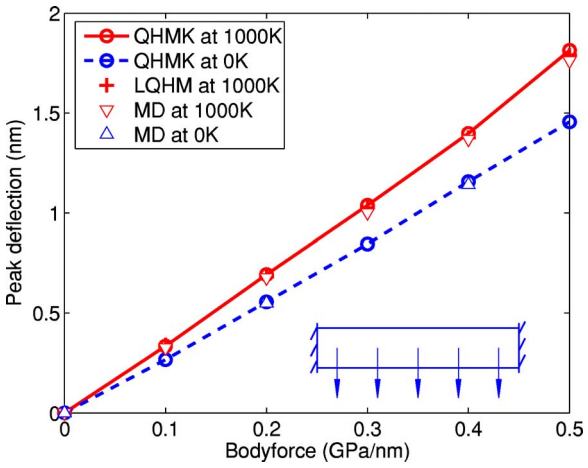

FIG. 8. (Color online) The peak displacement as a function of the applied body force (acts vertically downwards) for a fixed-fixed silicon beam at 0 and 1000 K.

atomic configuration of the surface atoms from that of the interior atoms, on the mechanical behavior of the nanostructure are typically negligible. However, when the characteristic length of the nanostructure is less than a few nanometers, the surface effects can become significant. The surface atomic configuration depends on the material as well as on the surrounding environment, which can be quite complicated for silicon nanostructures. In general, the Cauchy-Born rule may not hold for surface atoms. Accurate treatment of the surface atoms by the quasicontinuum method at finite temperatures is still an open research topic.[19,42] In this paper, we adopt a simple surface model, where the deformed configuration of the surface atoms is still assumed to follow the Cauchy-Born rule and the elastic properties at the surface are calculated by averaging over the first and the second layer of atoms. Although the surface model employed in this paper is simple, more advanced surface models can be readily incorporated in the finite-temperature QC framework. Figure 11 shows a $4\times10\times4$ unit cells, i.e., $2.173\times5.432\times2.173$ nm^3 (1487 atoms in MD simulations), silicon struc-

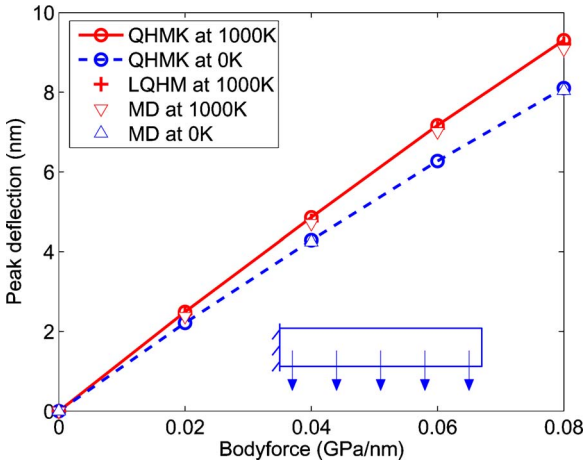

FIG. 9. (Color online) The peak displacement as a function of the applied body force (acts vertically downwards) for a cantilever silicon beam at 0 and 1000 K.

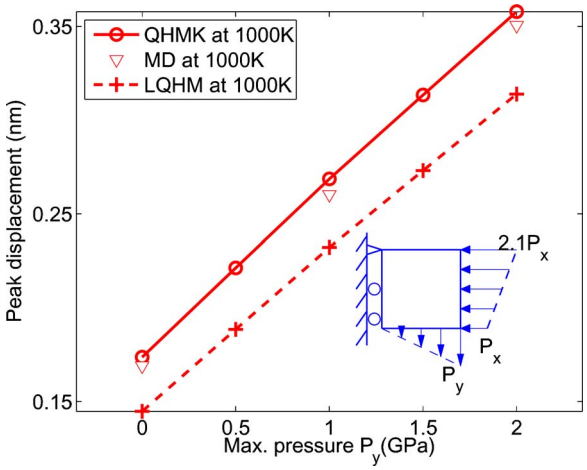

FIG. 10. (Color online) The peak displacement of a silicon beam subjected to a general loading at 1000 K. P_x=5 GPa and P_y varies from 0 to 2 GPa.

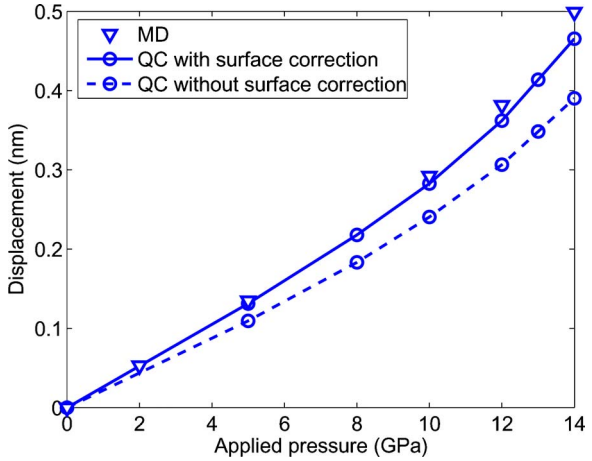

FIG. 12. (Color online) The displacement of point A shown in Fig. 11 as a function of the applied pressure.

ture with one end clamped and the other end subjected to a tensile pressure. The deformed shape of the nanostructure obtained from MD and the QC approaches (using the QHMK model) is compared. To investigate the significance of the surface effect, we also computed the deformed shape of the nanostructure without taking into account the surface effects, i.e., the surface atoms are treated the same as the interior atoms. As shown in Fig. 11, the primary local deformation features due to the surface effects are captured by the QC approach. Figure 12 shows the displacement as a function of the applied pressure for the corner point on the right surface of the structure shown in Fig. 11. The computed results compared well with the MD results.

V. CONCLUSIONS

We have proposed an extension of the original QC method to treat the solid structures at finite temperature. For isothermal systems at finite temperature, the constitutive relations are computed by using the Helmholtz free energy density. The static part of the Helmholtz free energy density is obtained directly from the interatomic potential while the vibrational part is calculated by using the real space quasiharmonic model, the local quasiharmonic model, and the **k**-space quasiharmonic model. Our results indicate that even though the real space quasiharmonic model predicts the material properties accurately, it is inefficient when the system contains more than several hundreds of atoms. The local quasiharmonic model is simple and efficient, but it can be inaccurate to predict elastic constants of Tersoff silicon, especially when the material is under strain. The **k**-space quasiharmonic model can predict the material properties accurately and efficiently. Using the finite-temperature QC method, we have investigated the effect of temperature and strain on the PDOS and phonon Grüneisen parameters, and calculated the elastic constants and the mechanical response of silicon nanostructures under external loads at various temperatures. Our results indicate that for silicon nanostructures larger than a few nanometers in critical dimension, the **k**-space quasiharmonic model predicts the mechanical response of the nanostructure accurately over a large temperature range, while the local quasiharmonic model can be inaccurate for Tersoff silicon.

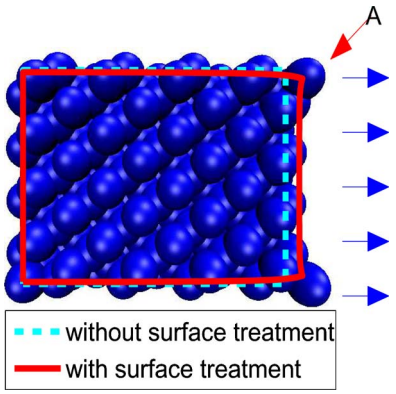

FIG. 11. (Color online) Deformed shape of a silicon nanostructure subjected to an axial pressure. Comparison of the MD and the QC approaches (874 K).

ACKNOWLEDGMENTS

We gratefully acknowledge support by the National Science Foundation under Grants No. 0103447, No. 0228390, No. 0403020, and No. 0519920.

APPENDIX A: CALCULATION OF THE DERIVATIVES OF THE BOND LENGTH AND BOND ANGLE

Given any two atoms α and β, the relative position vectors between their equilibrium positions in the initial and the deformed configurations are denoted by $\mathbf{R}^0_{\alpha\beta}$ and $\mathbf{r}^0_{\alpha\beta}$, respectively (see Fig. 1). Without losing generality, we assume $\alpha \in B_1$ and $\beta \in B_2$. From the Cauchy-Born rule, the two vectors are related by $\mathbf{r}^0_{\alpha\beta}=\mathbf{F}\mathbf{R}^0_{\alpha\beta}-\boldsymbol{\xi}$. The first derivatives of the bond length, $r^0_{\alpha\beta}=|\mathbf{r}^0_{\alpha\beta}|$, with respect to the deformation gradient $\mathbf{F}$ and the inner displacement $\boldsymbol{\xi}$, are given by

$$\frac{\partial r^0_{\alpha\beta}}{\partial \mathbf{F}_{ij}} = \frac{\mathbf{r}^0_{\alpha\beta i}}{r^0_{\alpha\beta}} \mathbf{R}^0_{\alpha\beta j}, \quad i,j = 1,2,3 \tag{A1}$$

and

$$\frac{\partial r^0_{\alpha\beta}}{\partial \boldsymbol{\xi}_i} = -\frac{\mathbf{r}^0_{\alpha\beta i}}{r^0_{\alpha\beta}}, \quad i = 1,2,3, \tag{A2}$$

where $\mathbf{r}^0_{\alpha\beta i}$ and $\mathbf{R}^0_{\alpha\beta j}$ are the ith and jth component of $\mathbf{r}^0_{\alpha\beta}$ and $\mathbf{R}^0_{\alpha\beta}$, respectively. The derivatives of $\cos\theta^0_{\alpha\beta\gamma}$ can be obtained by applying the chain rule, i.e.,

$$\frac{\partial \cos\theta^0_{\alpha\beta\gamma}}{\partial \mathbf{v}} = \left(\frac{1}{r^0_{\alpha\gamma}} - \frac{\cos\theta^0_{\alpha\beta\gamma}}{r^0_{\alpha\beta}}\right)\frac{\partial r^0_{\alpha\beta}}{\partial \mathbf{v}} + \left(\frac{1}{r^0_{\alpha\beta}} - \frac{\cos\theta^0_{\alpha\beta\gamma}}{r^0_{\alpha\gamma}}\right)\frac{\partial r^0_{\alpha\gamma}}{\partial \mathbf{v}} - \frac{r^0_{\beta\gamma}}{r^0_{\alpha\beta} r^0_{\alpha\gamma}}\frac{\partial r^0_{\beta\gamma}}{\partial \mathbf{v}}, \tag{A3}$$

where $\cos\theta^0_{\alpha\beta\gamma} = [(r^0_{\alpha\beta})^2 + (r^0_{\alpha\gamma})^2 - (r^0_{\beta\gamma})^2]/(2r^0_{\alpha\beta} r^0_{\alpha\gamma})$, and $\mathbf{v}$ can be $\mathbf{F}$ or $\boldsymbol{\xi}$.

The second derivatives of the bond length $r^0_{\alpha\beta}$ are given by

$$\frac{\partial^2 r^0_{\alpha\beta}}{\partial \mathbf{F}_{ij}\, \partial \mathbf{F}_{kl}} = \frac{\mathbf{R}^0_{\alpha\beta j}\mathbf{R}^0_{\alpha\beta l}}{r^0_{\alpha\beta}}\left(\delta_{ik} - \frac{\mathbf{r}^0_{\alpha\beta i}\mathbf{r}^0_{\alpha\beta k}}{(r^0_{\alpha\beta})^2}\right), \tag{A4}$$

$$\frac{\partial^2 r^0_{\alpha\beta}}{\partial \boldsymbol{\xi}_i\, \partial \boldsymbol{\xi}_j} = \frac{1}{r^0_{\alpha\beta}}\left(\delta_{ij} - \frac{\mathbf{r}^0_{\alpha\beta i}\mathbf{r}^0_{\alpha\beta j}}{(r^0_{\alpha\beta})^2}\right), \tag{A5}$$

$$\frac{\partial^2 r^0_{\alpha\beta}}{\partial \mathbf{F}_{ij}\, \partial \boldsymbol{\xi}_k} = -\frac{1}{r^0_{\alpha\beta}}\left(\delta_{ik} - \frac{\mathbf{r}^0_{\alpha\beta i}\mathbf{r}^0_{\alpha\beta k}}{(r^0_{\alpha\beta})^2}\right)\mathbf{R}^0_{\alpha\beta j}. \tag{A6}$$

The second derivatives of $\cos\theta^0_{\alpha\beta\gamma}$ are given by

$$\begin{aligned}\frac{\partial^2 \cos\theta^0_{\alpha\beta\gamma}}{\partial \mathbf{v}\, \partial \mathbf{w}} &= \left(\frac{1}{r^0_{\alpha\gamma}} - \frac{\cos\theta^0_{\alpha\beta\gamma}}{r^0_{\alpha\beta}}\right)\frac{\partial^2 r^0_{\alpha\beta}}{\partial \mathbf{v}\, \partial \mathbf{w}} \\ &+ \left(\frac{1}{r^0_{\alpha\beta}} - \frac{\cos\theta^0_{\alpha\beta\gamma}}{r^0_{\alpha\gamma}}\right)\frac{\partial^2 r^0_{\alpha\gamma}}{\partial \mathbf{v}\, \partial \mathbf{w}} - \frac{r^0_{\beta\gamma}}{r^0_{\alpha\beta} r^0_{\alpha\gamma}}\frac{\partial^2 r^0_{\beta\gamma}}{\partial \mathbf{v}\, \partial \mathbf{w}} \\ &+ \left(-\frac{1}{(r^0_{\alpha\gamma})^2}\frac{\partial r^0_{\alpha\gamma}}{\partial \mathbf{w}} - \frac{\partial \cos\theta^0_{\alpha\beta\gamma}}{\partial \mathbf{w}}\frac{1}{r^0_{\alpha\beta}} \right. \\ &\left. + \frac{\cos\theta^0_{\alpha\beta\gamma}}{(r^0_{\alpha\beta})^2}\frac{\partial r^0_{\alpha\beta}}{\partial \mathbf{w}}\right)\frac{\partial r^0_{\alpha\beta}}{\partial \mathbf{v}} \\ &+ \left(-\frac{1}{(r^0_{\alpha\beta})^2}\frac{\partial r^0_{\alpha\beta}}{\partial \mathbf{w}} - \frac{\partial \cos\theta^0_{\alpha\beta\gamma}}{\partial \mathbf{w}}\frac{1}{r^0_{\alpha\gamma}} \right. \\ &\left. + \frac{\cos\theta^0_{\alpha\beta\gamma}}{(r^0_{\alpha\gamma})^2}\frac{\partial r^0_{\alpha\gamma}}{\partial \mathbf{w}}\right)\frac{\partial r^0_{\alpha\gamma}}{\partial \mathbf{v}} \\ &+ \left(-\frac{1}{r^0_{\alpha\beta} r^0_{\alpha\gamma}}\frac{\partial r^0_{\beta\gamma}}{\partial \mathbf{w}} + \frac{r^0_{\beta\gamma}}{(r^0_{\alpha\beta})^2 r^0_{\alpha\gamma}}\frac{\partial r^0_{\alpha\beta}}{\partial \mathbf{w}} \right. \\ &\left. + \frac{r^0_{\beta\gamma}}{(r^0_{\alpha\gamma})^2 r^0_{\alpha\beta}}\frac{\partial r^0_{\alpha\gamma}}{\partial \mathbf{w}}\right)\frac{\partial r^0_{\beta\gamma}}{\partial \mathbf{v}},\end{aligned} \tag{A7}$$

where $\mathbf{v}$ and $\mathbf{w}$ could be $\mathbf{F}$ or $\boldsymbol{\xi}$.

APPENDIX B: EXPRESSION FOR ELASTIC CONSTANTS

Given the strain energy density W ($W = W_U$ for classical systems at zero temperature and $W = W_A$ for isothermal systems at finite temperature), the elastic constants are given by

$$\mathbf{C}_{ijkl} = \frac{\partial^2 W}{\partial \mathbf{E}_{ij}\, \partial \mathbf{E}_{kl}} - \frac{\partial^2 W}{\partial \mathbf{E}_{ij}\, \partial \boldsymbol{\xi}_m}\left(\frac{\partial^2 W}{\partial \boldsymbol{\xi}_m\, \partial \boldsymbol{\xi}_n}\right)^{-1}\frac{\partial^2 W}{\partial \boldsymbol{\xi}_n\, \partial \mathbf{E}_{kl}}, \quad i,j,k,l,m,n = 1,2,3. \tag{B1}$$

Noting that $\partial W/\partial \mathbf{F} = \mathbf{F}\,\partial W/\partial \mathbf{E}$ and $\partial W/\partial \mathbf{E} = \mathbf{F}^{-1}\partial W/\partial \mathbf{F}$, the second derivatives of W with respect to $\mathbf{E}_{ij}$ and $\mathbf{E}_{kl}$, $i,j,k,l = 1,2,3$, can be rewritten as the derivatives with respect to $\mathbf{F}$

$$\frac{\partial^2 W}{\partial \mathbf{E}_{ij}\, \partial \mathbf{E}_{kl}} = \mathbf{F}^{-1}_{in}\frac{\partial^2 W}{\partial \mathbf{F}_{nj}\, \partial \mathbf{F}_{mk}}\mathbf{F}^{-1}_{lm} - \mathbf{F}^{-1}_{in}\mathbf{F}^{-1}_{km}\frac{\partial W}{\partial \mathbf{F}_{mj}}\mathbf{F}^{-1}_{ln}. \tag{B2}$$

Substituting Eq. (B2) into Eq. (B1), we obtain the expression for the elastic constants in terms of $\mathbf{F}$ and $\boldsymbol{\xi}$, i.e.,

$$\begin{aligned}\mathbf{C}_{ijkl} &= \mathbf{F}^{-1}_{in}\frac{\partial^2 W}{\partial \mathbf{F}_{nj}\, \partial \mathbf{F}_{mk}}\mathbf{F}^{-1}_{lm} - \mathbf{F}^{-1}_{in}\mathbf{F}^{-1}_{km}\frac{\partial W}{\partial \mathbf{F}_{mj}}\mathbf{F}^{-1}_{ln} \\ &- \mathbf{F}^{-1}_{ip}\frac{\partial^2 W}{\partial \mathbf{F}_{pj}\, \partial \boldsymbol{\xi}_m}\left(\frac{\partial^2 W}{\partial \boldsymbol{\xi}_m\, \partial \boldsymbol{\xi}_n}\right)^{-1}\mathbf{F}^{-1}_{kq}\frac{\partial^2 W}{\partial \mathbf{F}_{ql}\, \partial \boldsymbol{\xi}_n},\end{aligned} \quad i,j,k,l,m,n,p,q = 1,2,3. \tag{B3}$$

APPENDIX C: DERIVATIVES OF VIBRATIONAL FREQUENCIES

As discussed in Sec. II D, to compute the elastic constants and the second Piola-Kirchhoff stress tensor, one needs to calculate the derivatives of the vibrational frequencies, ω_n, with respect to the deformation gradient $\mathbf{F}$ and the inner displacement $\boldsymbol{\xi}$. These calculations are not trivial because, first, degeneracies exist for the vibrational frequencies for a given wave vector $\mathbf{k}$ and the derivatives of the eigenvalues cannot be obtained directly from the Hellmann-Feynman theory;[43] second, the second derivatives, including the cross derivatives of ω_n with respect to $\mathbf{F}$ and $\boldsymbol{\xi}$, are required. The calculation becomes more involved when degeneracies occur in the first derivatives of ω_n. In this paper, we adopt the method proposed in Refs. 44–46. The method is summarized below.

Consider an $n \times n$ eigenvalue problem

$$\mathbf{D}\boldsymbol{\phi}_i = \lambda_i \boldsymbol{\phi}_i, \quad i = 1, \ldots, n. \tag{C1}$$

Without losing generality, we assume Eq. (C1) has a repeated root of order m and the eigenvalues are ordered so that $\lambda_1 = \lambda_2 = , \ldots, = \lambda_m$. The eigenvectors $\boldsymbol{\phi}_1, \boldsymbol{\phi}_2, \ldots, \boldsymbol{\phi}_m$ associated with this repeated eigenvalue are thus not unique, i.e., any linear combination of the eigenvectors is also an eigenvector. Assuming the eigenvectors are orthonormal vectors given by $\Phi = [\boldsymbol{\phi}_1, \boldsymbol{\phi}_2, \ldots, \boldsymbol{\phi}_m]$, then

$$\begin{aligned}\boldsymbol{\Psi} &= [\boldsymbol{\phi}_1, \boldsymbol{\phi}_2, \ldots, \boldsymbol{\phi}_m]_{n\times m}[\mathbf{h}_1\mathbf{h}_2, \ldots, \mathbf{h}_m]_{m\times m} \\ &= [\boldsymbol{\phi}_1, \boldsymbol{\phi}_2, \ldots, \boldsymbol{\phi}_m]\mathbf{H},\end{aligned} \tag{C2}$$

is also a set of orthonormal eigenvectors for any orthonormal

matrix $\mathbf{H}$, with $\psi_i = \Phi \mathbf{h}_i$. When the eigenvalue and eigenvector derivatives are required, the correct set of eigenvectors must be chosen, i.e., the correct $\mathbf{H}$ must be obtained. Differentiating Eq. (C1) with respect to a parameter θ_k by using ψ_i gives

$$\left(\frac{\partial \mathbf{D}}{\partial \theta_k} - \frac{\partial \lambda_i}{\partial \theta_k}\mathbf{I}\right)\psi_i + (\mathbf{D} - \lambda_i \mathbf{I})\frac{\partial \psi_i}{\partial \theta_k} = 0, \tag{C3}$$

and premultiplying by $\mathbf{\Phi}^H$, which is the Hermitian of $\mathbf{\Phi}$, one obtains

$$\Phi^H \frac{\partial \mathbf{D}}{\partial \theta_k}\Phi \mathbf{h}_i = \frac{\partial \lambda_i}{\partial \theta_k}\mathbf{h}_i. \tag{C4}$$

Note that Eq. (C4) is general. If there is no degeneracy for λ_i, then $\mathbf{h}_i$ is simply 1 and $\partial \lambda_i / \partial \theta_k$ can be obtained as the left-hand side of Eq. (C4). In the degenerate case, Eq. (C4) is an eigenvalue problem and the eigenvalue derivatives can be obtained. Differentiating Eq. (C3) with respect to a parameter θ_l and premultiplying by Φ^H gives

$$\Phi^H\left(\frac{\partial^2 \mathbf{D}}{\partial \theta_k \partial \theta_l} - \frac{\partial^2 \lambda_i}{\partial \theta_k \partial \theta_l}\mathbf{I}\right)\psi_i + \Phi^H\left(\frac{\partial \mathbf{D}}{\partial \theta_k} - \frac{\partial \lambda_i}{\partial \theta_k}\mathbf{I}\right)\frac{\partial \psi_i}{\partial \theta_l} + \Phi^H\left(\frac{\partial \mathbf{D}}{\partial \theta_l} - \frac{\partial \lambda_i}{\partial \theta_l}\mathbf{I}\right)\frac{\partial \psi_i}{\partial \theta_k} = 0, \tag{C5}$$

where, in general, the first derivative of ψ_i can be written as[44–46] $\partial \psi_i / \partial \theta_k = \mathbf{v}_{ki} + \Phi \mathbf{c}_{ki}$, where $\mathbf{v}_{ki}$ and $\mathbf{c}_{ki}$ are to be determined. Substituting $\partial \psi_i / \partial \theta_k$ into Eq. (C5), one obtains

$$\Phi^H\left(\frac{\partial^2 \mathbf{D}}{\partial \theta_k \partial \theta_l} - \frac{\partial^2 \lambda_i}{\partial \theta_k \partial \theta_l}\mathbf{I}\right)\psi_i + \Phi^H\left(\frac{\partial \mathbf{D}}{\partial \theta_k} - \frac{\partial \lambda_i}{\partial \theta_k}\mathbf{I}\right)\mathbf{v}_{li} + \Phi^H\left(\frac{\partial \mathbf{D}}{\partial \theta_l} - \frac{\partial \lambda_i}{\partial \theta_l}\mathbf{I}\right)\mathbf{v}_{ki} = 0, \tag{C6}$$

where $\mathbf{v}_{ki}$ is given by $\mathbf{v}_{ki} = \mathbf{V}_k \mathbf{h}_i$, and $\mathbf{V}_k$ is a solution of $(\mathbf{D} - \lambda \mathbf{I})\mathbf{V}_k = -(\partial \mathbf{D} / \partial \theta_k - \partial \lambda_i / \partial \theta_k \mathbf{I})\Phi$. Note that $(\mathbf{D} - \lambda \mathbf{I})$ is rank deficient with rank $(n-m)$. Therefore, m elements of each vector of $\mathbf{V}_k$ must be assigned. Several techniques can be employed to select m elements in the vectors of $\mathbf{V}_k$.[45] In this paper, we set the elements of the vectors of $\mathbf{V}_k$ corresponding to the m elements of the largest magnitude in each vector of Φ to be zero. Substituting $\mathbf{v}_{ki}$ into Eq. (C6) gives

$$\Phi^H\left(\frac{\partial^2 \mathbf{D}}{\partial \theta_k \partial \theta_l}\right)\Phi \mathbf{h}_i + \Phi^H\left(\frac{\partial \mathbf{D}}{\partial \theta_k} - \frac{\partial \lambda_i}{\partial \theta_k}\mathbf{I}\right)\mathbf{V}_l \mathbf{h}_i + \Phi^H\left(\frac{\partial \mathbf{D}}{\partial \theta_l} - \frac{\partial \lambda_i}{\partial \theta_l}\mathbf{I}\right)\mathbf{V}_k \mathbf{h}_i = \frac{\partial^2 \lambda_i}{\partial \theta_k \partial \theta_l}\mathbf{h}_i. \tag{C7}$$

By solving the eigenvalue problem, Eq. (C7), the second derivatives of the eigenvalues can be obtained.

[1] H. G. Craighead, Science **290**, 1532 (2000).
[2] Y. T. Yang, K. L. Ekinci, X. M. H. Huang, L. M. Schiavone, M. L. Roukes, C. A. Zorman, and M. Mehregany, Appl. Phys. Lett. **78**, 162 (2001).
[3] L. Pescini, H. Lorenz, and R. H. Blick, Appl. Phys. Lett. **82**, 352 (2003).
[4] M. Dequesnes, S. Rotkin, and N. R. Aluru, Nanotechnology **13**, 120 (2002).
[5] Z. Tang, Y. Xu, G. Li, and N. R. Aluru, J. Appl. Phys. **97**, 114304 (2005).
[6] J. Q. Broughton, F. F. Abraham, N. Bernstein, and E. Kaxiras, Phys. Rev. B **60**, 2391 (1999).
[7] O. Atkas and N. R. Aluru, J. Comput. Phys. **178**, 342 (2002).
[8] M. Dequesnes, Z. Tang, and N. R. Aluru, J. Eng. Mater. Technol. **126**, 230 (2004).
[9] P. A. Deymier and J. O. Vasseur, Phys. Rev. B **66**, 134106 (2002).
[10] T. Belytschko and S. P. Xiao, Int. J. Multiscale Comp. Eng. **1**, 115 (2003).
[11] E. B. Tadmor, M. Ortiz, and R. Philips, Philos. Mag. A **73**, 1529 (1996).
[12] E. B. Tadmor, G. S. Smith, N. Bernstein, and E. Kaxiras, Phys. Rev. B **59**, 235 (1999).
[13] V. B. Shenoy, R. Miller, E. B. Tadmor, D. Rodney, R. Phillips, and M. Ortiz, J. Mech. Phys. Solids **47**, 611 (1999).
[14] G. J. Wagner and W. K. Liu, J. Comput. Phys. **190**, 249 (2003); E. G. Karpov, G. J. Wagner, and W. K. Liu, Int. J. Numer. Methods Eng. **62**, 1250 (2005); H. S. Park, E. G. Karpov, P. A. Klein, and W. K. Liu, Philos. Mag. **85**, 79 (2005).
[15] E. Weinan, B. Engquist, and Z. Huang, Phys. Rev. B **67**, 092101 (2003).
[16] R. E. Rudd and J. Q. Broughton, Phys. Rev. B **58**, R5893 (1998).
[17] J. Fish and W. Chen, Comput. Methods Appl. Mech. Eng. **193**, 1693 (2004).
[18] V. Shenoy, V. Shenoy, and R. Phillips, Mater. Res. Soc. Symp. Proc. **538**, 465 (1999).
[19] R. E. Miller and E. B. Tadmor, J. Comput.-Aided Mater. Des. **9**, 203 (2002).
[20] H. Jiang, Y. Huang, and K. C. Hwang, J. Eng. Mater. Technol. **127**, 408 (2005).
[21] L. M. Dupuy, E. B. Tadmor, R. E. Miller, and R. Phillips, Phys. Rev. Lett. **95**, 060202 (2005).
[22] R. LeSar, R. Najafabadi, and D. J. Srolovitz, Phys. Rev. Lett. **63**, 624 (1989).
[23] J. Tersoff, Phys. Rev. B **38**, 9902 (1988).
[24] W. A. Harrison, *Electronic Structure and the Properties of Solids* (Freeman, San Francisco, 1980).
[25] M. Born and K. Huang, *Dynamical Theory of Crystal Lattices* (Clarendon, Oxford, 1954).
[26] D. C. Wallace, *Thermodynamics of Crystals* (John Wiley & Sons, New York, 1972).
[27] L. E. Malvern, *Introduction to the Mechanics of Continuum Medium* (Prentice-Hall, Englewood Cliffs, NJ, 1969).

[28] H. Balamane, T. Halicioglu, and W. A. Tiller, Phys. Rev. B **46**, 2250 (1992).
[29] H. Zhao, Z. Tang, G. Li, and N. R. Aluru, J. Appl. Phys. **99**, 064314 (2006).
[30] N. R. Aluru and G. Li, Int. J. Numer. Methods Eng. **50**, 2373 (2001).
[31] N. W. Ashcroft and N. D. Mermin, *Solid State Physics* (Holt-Saunders, Tokyo, Japan, 1981).
[32] F. Bloch, Z. Phys. **52**, 555 (1928).
[33] W. G. Hoover, Phys. Rev. A **31**, 1695 (1985).
[34] M. P. Allen and D. J. Tildesley, *Computer Simulation of Liquid* (Clarendon, Oxford, 1987).
[35] C. Z. Wang, C. T. Chan, and K. M. Ho, Phys. Rev. B **42**, 11276 (1990).
[36] A. A. Maradudin, E. W. Montroll, G. H. Weiss, and I. P. Ipatova, *Theory of Lattice Dynamics in the Harmonic Approximation* (Academic, New York, 1971).
[37] L. J. Porter, S. Yip, M. Yamaguchi, H. Kaburaki, and M. Tang, J. Appl. Phys. **81**, 96 (1997).
[38] A. P. Boresi and P. P. Lynn, *Elasticity in Engineering Mechanics* (Prentice-Hall, Englewood Cliffs, NJ, 1974).
[39] J. Tersoff, Phys. Rev. B **37**, 6991 (1988).
[40] S. Izumi and S. Sakai, JSME Int. J., Ser. A **47**, 54 (2004).
[41] M. Karimi, H. Yates, J. R. Ray, T. Kaplan, and M. Mostoller, Phys. Rev. B **58**, 6019 (1998).
[42] V. B. Shenoy, R. Miller, E. B. Tadmor, R. Phillips, and M. Ortiz, Phys. Rev. Lett. **80**, 742 (1998).
[43] R. P. Feynman, Phys. Rev. **56**, 340 (1939).
[44] W. C. Mills-Curran, AIAA J. **26**, 867 (1988).
[45] M. I. Friswell, J. Vibr. Acoust. **118**, 390 (1996).
[46] U. Prells and M. I. Friswell, AIAA J. **35**, 1363 (1997).